

Two-particle transverse momentum correlations in pp and p-Pb collisions at energies available at the CERN Large Hadron Collider

Original

Two-particle transverse momentum correlations in pp and p-Pb collisions at energies available at the CERN Large Hadron Collider / Acharya, S., Adamová, D., Adler, A., Aglieri Rinella, G., Agnello, M., Agrawal, N., Ahammed, Z., Ahmad, S., Ahn, S.U., Ahuja, I., Akindinov, A., Al-Turany, M., Aleksandrov, D., Alessandro, B., Alfanda, H.M., Alfaro Molina, R., Ali, B., Alici, A., Alizadehvandchali, N., Alkin, A., et al.. - In: PHYSICAL REVIEW C. - ISSN 2469-9985. - STAMPA. - 107:5(2023), pp. 1-20. [10.1103/PhysRevC.107.054617]

Availability:

This version is available at: 11583/2990258 since: 2024-07-02T18:36:08Z

Publisher:

American Physical Society

Published

DOI:10.1103/PhysRevC.107.054617

Terms of use:


This article is made available under terms and conditions as specified in the corresponding bibliographic description in the repository

Publisher copyright

(Article begins on next page)

Two-particle transverse momentum correlations in pp and p -Pb collisions at energies available at the CERN Large Hadron Collider

S. Acharya *et al.**
(ALICE Collaboration)

 (Received 23 November 2022; accepted 25 January 2023; published 30 May 2023)

Two-particle transverse momentum differential correlators, recently measured in Pb-Pb collisions at energies available at the CERN Large Hadron Collider (LHC), provide an additional tool to gain insights into particle production mechanisms and infer transport properties, such as the ratio of shear viscosity to entropy density, of the medium created in Pb-Pb collisions. The longitudinal long-range correlations and the large azimuthal anisotropy measured at low transverse momenta in small collision systems, namely pp and p -Pb, at LHC energies resemble manifestations of collective behavior. This suggests that locally equilibrated matter may be produced in these small collision systems, similar to what is observed in Pb-Pb collisions. In this work, the same two-particle transverse momentum differential correlators are exploited in pp and p -Pb collisions at $\sqrt{s} = 7$ TeV and $\sqrt{s_{NN}} = 5.02$ TeV, respectively, to seek evidence for viscous effects. Specifically, the strength and shape of the correlators are studied as a function of the produced particle multiplicity to identify evidence for longitudinal broadening that might reveal the presence of viscous effects in these smaller systems. The measured correlators and their evolution from pp and p -Pb to Pb-Pb collisions are additionally compared to predictions from Monte Carlo event generators, and the potential presence of viscous effects is discussed.

DOI: [10.1103/PhysRevC.107.054617](https://doi.org/10.1103/PhysRevC.107.054617)

I. INTRODUCTION

Studies at the Large Hadron Collider (LHC) and the Relativistic Heavy-Ion Collider (RHIC) have shown that quark-gluon plasma (QGP) matter is produced in relativistic collisions of large nuclei [1–11], and considerable efforts have been undertaken to measure some of the key properties of this phase of matter. One such property, the shear viscosity per unit entropy density, η/s , has received much attention from both the theoretical and experimental communities [12–17]. Measurements of anisotropic flow coefficients as well as symmetric cumulants, which are correlations between flow coefficients of different orders, in particular, have been successfully exploited to determine the extent to which the QGP is an almost perfect fluid, and many advances have been accomplished in improving estimates of the QGP η/s based on such measurements [18–20].

A new line of investigation was recently undertaken to extract values of the QGP η/s . This approach is based on measurements of the longitudinal broadening of a specific type of transverse momentum differential two-particle correlation function known as G_2 in the recent literature [21–23]. While the technique is relatively new and still needs to be fully vetted

by detailed (3+1)-dimensional hydrodynamical calculations, a recent measurement of the longitudinal broadening of G_2 in central Pb-Pb collisions, by the ALICE Collaboration [24], is found to yield an η/s range compatible with estimations based on anisotropic flow [25]. This agreement suggests that the new approach has merits and potential in furthering the understanding of the properties of QGP matter produced in collisions of large nuclei.

In proton-proton (pp) and proton-lead (p -Pb) collisions, femtoscopy radii, related to the estimated size of the system, and average transverse momentum, $\langle p_T \rangle$, increase with the multiplicity of produced particles [26–30], which implies that the system lives longer as the multiplicity increases, i. e., as the system size increases. In turn, this means that radial flow would have more time to develop. In these terms, for a given system size, viscous effects, if present, will have a certain time to manifest themselves by transferring momentum between neighboring fluid cells. This transfer of momentum will make the correlation function for that system size acquire, at the end, a certain longitudinal width which reflects the reach of the viscous effects. With larger multiplicity, the larger the system size is and the larger the time the system lives, the reach of the viscous effects will also be larger, which causes the longitudinal width of the correlation function to enlarge. Overall, the correlation function broadens longitudinally with the system size, the system lifetime, and the system multiplicity. In contrast, as more radial flow builds up with increasing multiplicity, system size, and lifetime, a narrower width is expected in the correlator azimuthal dimension. The fact that viscous effects are, in principle, independent of the charge and that radial flow has a strong charge dependent component

*Full author list given at the end of the article.

Published by the American Physical Society under the terms of the [Creative Commons Attribution 4.0 International](https://creativecommons.org/licenses/by/4.0/) license. Further distribution of this work must maintain attribution to the author(s) and the published article's title, journal citation, and DOI.

[31,32] implies that the charge independent (CI) and charge dependent (CD) correlators play complementary roles in the evaluation of the interplay between these effects.

It is thus natural to consider whether the above technique could also be exploited in the study of small systems, such as proton-proton (pp) and proton-lead (p -Pb) collisions. Measurements of anisotropic flow coefficients and multi-particle cumulants indicate that strong collective behavior exists in high-multiplicity pp and p -Pb collisions [33–35]. Several calculations based on hydrodynamics models [36,37] suggest that the observed coefficients can in fact be interpreted as evidence of collective flow in high multiplicity pp and p -Pb collisions. An important question is whether the apparent collectivity arises from the production of a medium, albeit much smaller than that produced in Pb-Pb collisions, or is due to other types of correlation sources.

In this context, it is of interest to examine whether measurements of G_2 in small collision systems can be exploited to identify the existence of a droplet sufficiently large and long lived such that viscous effects can yield a longitudinal broadening of the correlator. A particularly appealing aspect of the G_2 correlator is that it can be studied for charge dependent and charge independent pairs of particles. The charge independent G_2 correlator, hereafter denoted G_2^{CI} , is by construction sensitive to momentum current correlations. It is thus expected to exhibit a progressive broadening from small to large multiplicity collisions if these involve a long lived QGP matter undergoing both longitudinal and transverse expansion. In this expansion, shear viscous effects can transform stochastic radial currents and produce a longitudinal broadening of the correlator. However, the shape and evolution of G_2^{CI} may also be impacted by the presence of hadronic decays and radial flow and by minijet correlations resulting from parton shower evolution, string-breaking, and hadronization effects. Measurements of the charge dependent G_2 correlator, hereafter noted G_2^{CD} , can be exploited to specifically study these contributions. Indeed, G_2^{CD} and other two-particle differential correlation functions are found to be particularly sensitive to the presence of hadronic resonance decays and radial flow,

but somewhat less sensitive to shear viscous effects [38,39]. They can thus, in principle, be used to assess these effects and “calibrate them” out of measurements of G_2^{CI} .

Prior measurements of two-particle azimuthal correlations in the p -Pb system [40] compared the strengths of azimuthal modulations in collisions producing the largest and lowest charged particle multiplicities. They found evidence of sizable flowlike azimuthal correlation structures in high-multiplicity p -Pb collisions but did not study their pseudorapidity dependence in detail. It is thus the primary goal of this work to extend those correlation studies and measure the evolution of G_2^{CD} and G_2^{CI} as a function of the produced charged particle multiplicity in both pp and p -Pb collisions. Then, this will allow seeking evidence for longitudinal broadening of G_2^{CI} signaling viscous effects that should happen if relatively long lived QGP matter is produced in these collisions.

This work is organized as follows. Section II defines the two-particle correlator G_2 and presents the measurement methodology, while Sec. III describes the experimental details and corrections applied to the data. Section IV presents the techniques used to determine statistical and systematic uncertainties on the measured correlation function amplitudes and their characteristics, reported in Sec. V. The method used to characterize the shape of the correlation functions and its evolution with multiplicity is presented in Sec. VI. Measurements of the evolution of the longitudinal and azimuthal widths of the correlators are compared to model calculations in Sec. VII. A discussion of the results and models is presented in Sec. VIII followed by a summary of the conclusions of this work in Sec. IX.

II. ANALYSIS METHODOLOGY

The G_2 correlator is designed to be proportional to the magnitude of momentum currents, the transferring of momentum fluctuations, and their correlations, from which viscous effects can be inferred [21,22]. It is defined as

$$G_2(\eta_1, \varphi_1, \eta_2, \varphi_2) = \frac{1}{\langle p_{T,1} \rangle \langle p_{T,2} \rangle} \left[\frac{\int_{\Omega} p_{T,1} p_{T,2} \rho_2(\vec{p}_1, \vec{p}_2) d p_{T,1} d p_{T,2}}{\int_{\Omega} \rho_1(\vec{p}_1) d p_{T,1} \int_{\Omega} \rho_1(\vec{p}_2) d p_{T,2}} - \langle p_{T,1} \rangle \langle p_{T,2} \rangle \right], \quad (1)$$

where $\rho_1(\vec{p}_i)$ and $\rho_2(\vec{p}_1, \vec{p}_2)$ represent single-particle and pair densities computed as

$$\rho_1(\vec{p}_i) = \frac{d^3 N}{d p_{T,i} d \eta_i d \varphi_i}, \quad (2)$$

$$\rho_2(\vec{p}_1, \vec{p}_2) = \frac{d^6 N}{d p_{T,1} d \eta_1 d \varphi_1 d p_{T,2} d \eta_2 d \varphi_2}, \quad (3)$$

with particle three-momenta $\vec{p}_i = (\eta_i, \varphi_i, p_{T,i})$ and components $\eta_i, \varphi_i, p_{T,i}$ corresponding to the pseudorapidity, azimuthal angle, and transverse momentum of particles $i = 1, 2$, composing pairs. Transverse momentum averages $\langle p_{T,i} \rangle$ are

calculated according to

$$\langle p_{T,i} \rangle(\eta_i, \varphi_i) = \frac{\int_{\Omega} \rho_1(\eta_i, \varphi_i, p_{T,i}) p_{T,i} d p_{T,i}}{\int_{\Omega} \rho_1(\eta_i, \varphi_i, p_{T,i}) d p_{T,i}}. \quad (4)$$

Integrals are computed in the measurement acceptance Ω . Measurements of $G_2(\eta_1, \varphi_1, \eta_2, \varphi_2)$ are averaged across the longitudinal and azimuthal acceptances in which the measurement is performed to obtain $G_2(\Delta\eta, \Delta\varphi)$, where $\Delta\eta = \eta_1 - \eta_2$ and $\Delta\varphi = \varphi_1 - \varphi_2$, with a procedure similar to that used for the two-particle number correlator R_2 and the two-particle transverse momentum correlator P_2 [32], as well as for measurements of G_2 in Pb-Pb collisions [24].

In order to account for distinct efficiency losses associated with positively (+) and negatively (−) charged particles, G_2 correlators are first measured for pairs of (++) , (−−) , (−+), and (+−) charged hadrons. These measurements are combined to yield like-sign (LS) and unlike-sign (US) pairs correlators $G_2^{LS} = \frac{1}{2}(G_2^{++} + G_2^{--})$ and $G_2^{US} = \frac{1}{2}(G_2^{+-} + G_2^{-+})$. In turn, these are further combined to obtain the charge dependent and the charge independent correlators defined as $G_2^{CD} = \frac{1}{2}(G_2^{US} - G_2^{LS})$ and $G_2^{CI} = \frac{1}{2}(G_2^{US} + G_2^{LS})$, respectively [32].

The G_2^{CD} and G_2^{CI} correlators are measured in pp and p -Pb collisions using event classes based on the average charged particle multiplicity detected at forward pseudorapidities. The multiplicity evolution of the shape and strength of these correlators is then extracted and analyzed as described in Sec. VI.

III. DATASETS AND EXPERIMENTAL SETUP

The results presented in this article are based on 6.4×10^7 selected minimum bias (MB) pp collisions at center-of-mass energy $\sqrt{s} = 7$ TeV and 5.4×10^7 selected MB p -Pb collisions at center-of-mass energy per nucleon-nucleon collision $\sqrt{s_{NN}} = 5.02$ TeV collected during the 2010 and 2013 LHC runs, respectively, with the ALICE detector. Detailed descriptions of the ALICE subsystems and their respective performance are given in Refs. [41,42].

The MB trigger was configured to provide a high efficiency for hadronic events. It required coincident signals in the V0A and V0C scintillator arrays [43], covering the pseudorapidity ranges $2.8 < \eta < 5.1$ and $-3.7 < \eta < -1.7$, respectively. Calibrated SPD and V0 signal amplitudes were used to estimate the charged particle multiplicity production in these pseudorapidity ranges. The resulting multiplicity distribution was used to establish nine multiplicity classes corresponding to 0–5% (highest multiplicity), 5–10%, 10–20%, 20–30%, 30–40%, 40–50%, 50–60%, 60–70%, and 70–80% (lowest multiplicity) of the inelastic cross section. The correlators G_2^{CI} and G_2^{CD} are extracted independently in each of these multiplicity classes and the evolution of their widths is reported as a function of the average number of charged particles [N_{ch}] measured in the fiducial acceptance of the measurement.

The collision vertex position of each event, called primary vertex (PV), is determined from the charged particle tracks reconstructed in the Inner Tracking System (ITS) and the Time Projection Chamber (TPC). Only events with a reconstructed PV position within 7 cm from the nominal interaction point along the beam direction were included in the analysis. Background events from beam interactions with residual gas in the beam pipe are removed using the timing information in the V0. Pileup events having multiple interaction vertices are discarded based on information from the Silicon Pixel Detector (SPD) constituting the two inner layers of the ITS. Extra activity in slow response detectors (e. g., TPC) relative to that in fast detectors (e. g., V0A and V0C scintillators) resulting largely from out-of-bunch pileup events, is additionally used to discard these events.

Charged particle tracks are reconstructed using the ITS and TPC detectors and required to have transverse momenta and pseudorapidities within the ranges $0.2 \leq p_T \leq 2.0$ GeV/ c

and $|\eta| < 0.8$, respectively. Good track quality is assured by retaining only tracks with more than 70 reconstructed TPC space points, out of a maximum of 159, for the analysis. A criterion on the maximum distance of closest approach (DCA) to the reconstructed PV of less than 2 cm in the longitudinal dimension and a p_T dependent maximum DCA in the transverse direction, ranging from 0.20 cm at $p_T = 0.2$ GeV/ c down to 0.036 cm at $p_T = 2$ GeV/ c for pp collisions and from 0.22 cm at $p_T = 0.2$ GeV/ c down to 0.031 cm at $p_T = 2$ GeV/ c for p -Pb collisions, is applied to minimize contamination by secondary tracks. Moreover, electrons (positrons), which originate mainly from photon conversions into e^+e^- pairs, are suppressed by removing tracks with a specific energy loss in the TPC gas, dE/dx , within three standard deviations, $3\sigma_{dE/dx}$, of the expected value for electrons and more than $5\sigma_{dE/dx}$ away from the π and K expectation values.

Corrections for single track losses due to detector nonuniformity are based on a weighting technique [44]. Weights are calculated separately for positive and negative tracks as a function of η , ϕ , and p_T and averaged across the measured ranges of multiplicity and primary vertex position. Weights are used to flatten the track yield in both pseudorapidity and in azimuth for the symmetric collision system, pp , whereas only azimuthal flattening is used for p -Pb collisions.

Corrections for tracking inefficiencies are obtained from Monte Carlo simulations with different event generators and particle transport through the detector performed with GEANT3 [45] including a detailed description of the detector conditions during the 2010 and 2013 data taking periods. Simulations with the PYTHIA 6 event generator [46] (Perugia 2011 tune [47]) are used to determine the track reconstruction efficiency for the data sample of pp collisions. For the p -Pb system, the DPMJET event generator [48] is used. The p_T and η dependence of the single-particle detection efficiency is computed based on the ratio of the number of reconstructed tracks from the simulation (known as detector level), corrected for the nonuniformity of the detector (weights), to the number of generated particles (known as generator level) as a function of those two variables. Reconstructed tracks from the data sample are corrected for detector nonuniformity and for tracking inefficiencies for extracting the described corrected correlators. The number of fully corrected measured charged tracks is averaged over the number of events to extract the quoted [N_{ch}] per multiplicity class.

IV. STATISTICAL AND SYSTEMATIC UNCERTAINTIES

The statistical uncertainties on the strengths of the G_2 correlators are extracted with the subsampling method using ten subsamples for both systems, pp and p -Pb, whereas systematic uncertainties are assessed by repeating the analysis with different event and track selection criteria. The significance of the deviations with respect to the default analysis conditions is assessed according to a statistical test [49]. The total systematic uncertainties are computed as quadratic sums of the significant systematic deviations. The contributions to the uncertainty due to the event selection and the kinematic acceptance are estimated by narrowing to 3 cm and expanding to 10 cm the selected range for the distance of the PV to the

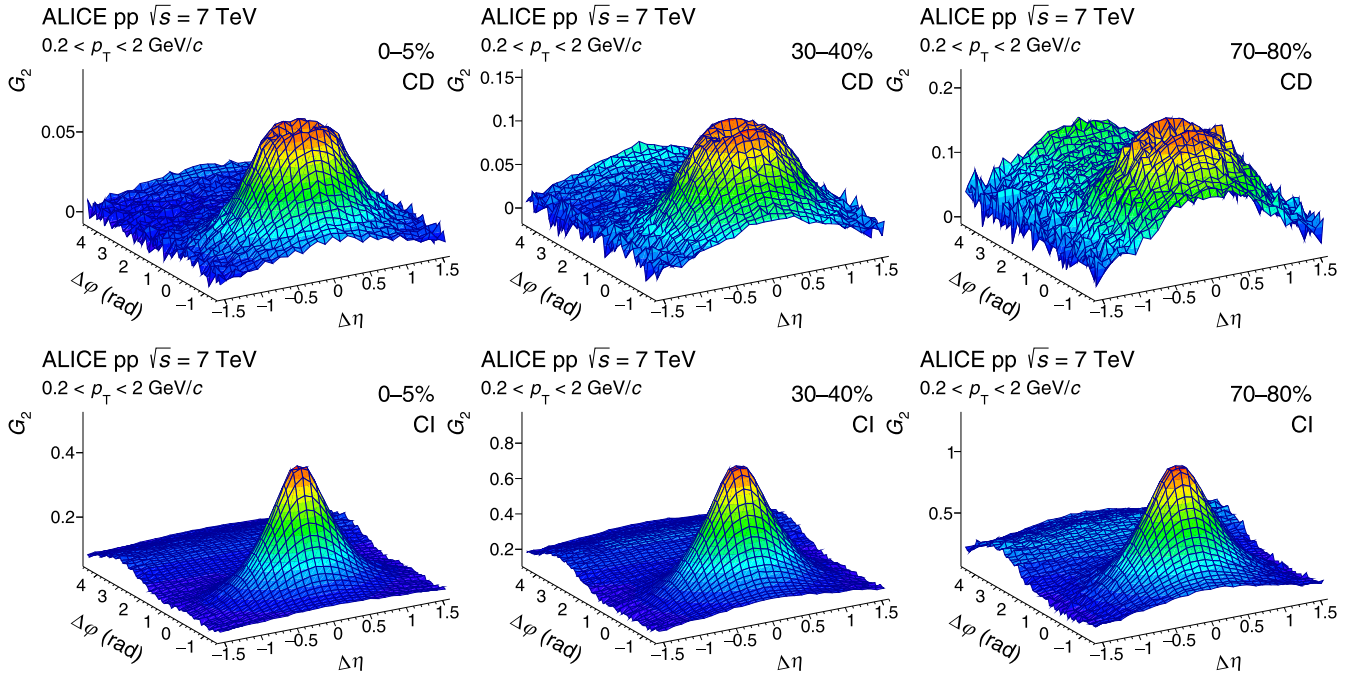


FIG. 1. Two-particle transverse momentum correlations G_2^{CD} (top) and G_2^{CI} (bottom) for the largest (left), medium (center), and lowest (right) charged particle multiplicity classes in pp collisions at $\sqrt{s} = 7$ TeV. The correlator values are not shown in the intervals $|\Delta\eta| < 0.1$ and $|\Delta\phi| < 0.09$, which are affected by track merging effects (see text for details).

nominal interaction point along the beam direction. Possible biases associated with contamination by secondary particles are estimated by using track selection criteria that only require information from the TPC and relaxing the accepted DCA range. The possible biases in the determination of the track parameters for tracks crossing the TPC in the azimuthal regions close to the sector boundaries is estimated by excluding tracks that lie within those sections from the analysis. This additional selection criterion eliminates distortions possibly encountered near sector boundaries but produces a nominal 25% reduction of the azimuthal acceptance. Track losses are, however, compensated for by the robust nature of the G_2 correlator definition as a ratio of two-particle density to the product of single-particle densities. The overall accuracy of the analysis procedure is additionally estimated by means of a MC closure test. Deviations from perfect closure are conservatively added to systematic uncertainties when significant. The same criteria are followed to extract the statistical and systematic uncertainties on $[N_{\text{ch}}]$.

As in the study of G_2 in Pb-Pb collisions reported in Ref. [24], measurements of the G_2 longitudinal and azimuthal projections in pp and p -Pb collisions feature an overall amplitude uncertainty. This uncertainty includes correlated (i. e., common to all bins) and uncorrelated bin-by-bin contributions. The correlated contribution is the average deviation along all bins while the uncorrelated contribution is what remains after subtracting such average from the actual deviation on a per bin basis. The largest contribution to the correlated systematic uncertainties arises from the variation of the track selection criteria with an average value in the different multiplicity classes of 10% (4%) for both the longitudinal and the azimuthal projections of the G_2^{CD} (G_2^{CI}) correlator in the pp

system, and about 12% (1.5%) for both the longitudinal and the azimuthal projections in p -Pb collisions, while the other checks have negligible contributions. The largest systematic contribution to the uncorrelated uncertainty also stems from track selection criteria tests with average values of 6% (1.5%) for both the longitudinal and the azimuthal projections of the G_2^{CD} (G_2^{CI}) correlator in the pp system, and less than 9% (1%) in the p -Pb system. Total average uncorrelated systematic uncertainties values are approximately the same for the azimuthal and longitudinal projections except for the azimuthal projections of the G_2^{CD} correlator in the p -Pb system, which reach 12% due to the impact of the TPC sector boundaries.

V. RESULTS

The G_2^{CD} and G_2^{CI} correlators measured in pp collisions at $\sqrt{s} = 7$ TeV and p -Pb collisions at $\sqrt{s_{\text{NN}}} = 5.02$ TeV are shown in Figs. 1 and 2, respectively, for three selected multiplicity classes, as functions of the pair separation in pseudorapidity $\Delta\eta$ and azimuth $\Delta\phi$. The G_2^{CD} and G_2^{CI} correlators exhibit common features in both pp and p -Pb collisions. Such features include a prominent peak centered at $\Delta\eta = 0$, $\Delta\phi = 0$, hereafter referred to as the near-side peak, and a relatively flat plateau shaped distribution surrounding $\Delta\phi = \pi$, known as the away side, and extending across the $\Delta\eta$ acceptance of the measurement. The near-side peak of both G_2^{CD} and G_2^{CI} exhibits a monotonically decreasing amplitude from the lowest to the highest multiplicity classes, in both collision systems, while the peak shapes are approximately independent of the collision multiplicity. It is also observed that the away-side amplitude of the G_2^{CD} correlator measured in pp collisions decreases somewhat faster than that of the

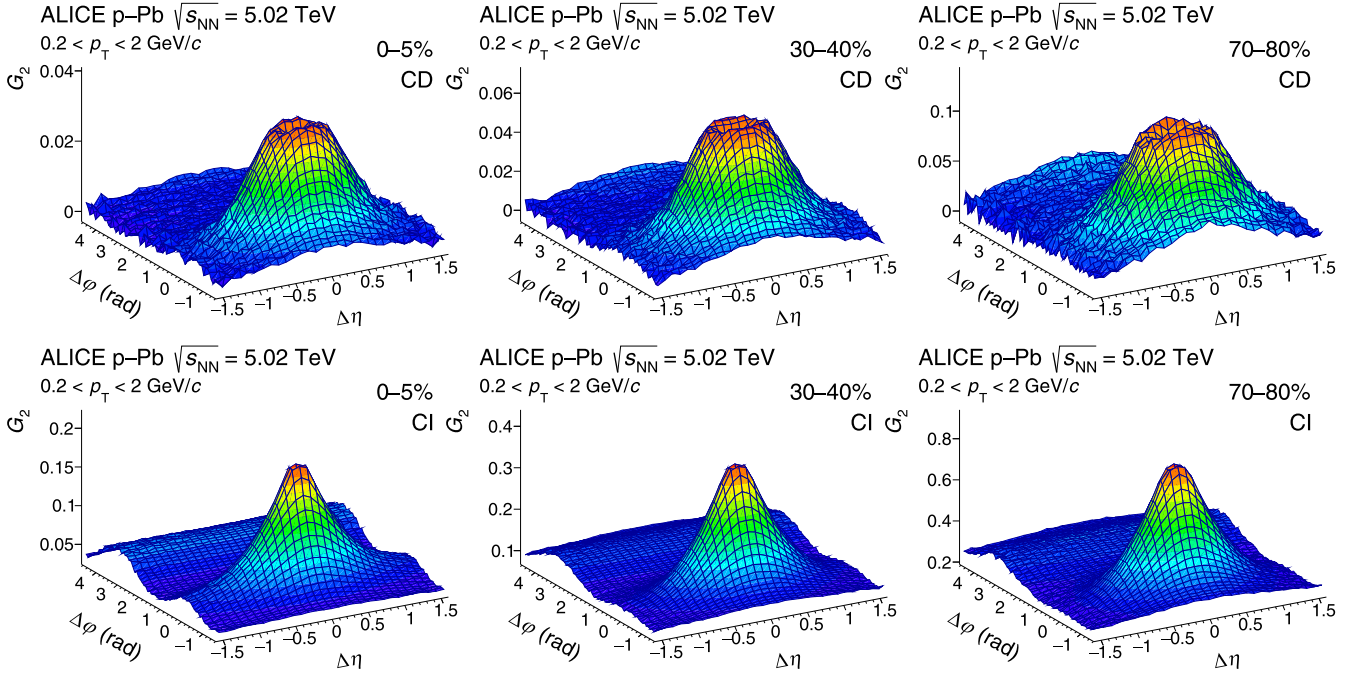


FIG. 2. Two-particle transverse momentum correlations G_2^{CD} (top) and G_2^{CI} (bottom) for the largest (left), medium (center), and lowest (right) charged particle multiplicity classes in p -Pb collisions at $\sqrt{s_{\text{NN}}} = 5.02$ TeV. The correlator values are not shown in the intervals $|\Delta\eta| < 0.1$ and $|\Delta\phi| < 0.09$, which are affected by track merging effects (see text for details).

near-side peak, whereas the shape of the away side of the G_2^{CI} correlators exhibits only modest variations with multiplicity.

Additionally, the G_2^{CI} correlators measured in p -Pb collisions feature a modest azimuthal modulation approximately uniform in magnitude across the $\Delta\eta$ range of the measurement. The modulation is expected from prior ALICE azimuthal correlation measurements [40] but is observed in greater detail in Fig. 2. Remarkably, also the near-side peak of the CD correlator in p -Pb collisions does not appear to narrow significantly with increasing multiplicity in contrast with the behavior observed in the pp system.

Further examination of the evolution of the correlators as a function of the produced particle multiplicity is done by studying their longitudinal and azimuthal projections. The longitudinal projections, shown in the left panels of Figs. 3 and 4 for the pp and p -Pb systems, respectively, display the average of the G_2 correlators as a function of $\Delta\eta$ for the near-side azimuthal interval $|\Delta\phi| < \pi/2$ whereas the azimuthal projections (right panels) are obtained by averaging the correlators over the full $\Delta\eta$ range of the measurements. The ranges $|\Delta\eta| < 0.1$ and $|\Delta\phi| < 0.09$ are subject to track merging effects difficult to properly correct for and are thus omitted in the projection plots. The longitudinal projections of the CI correlators (bottom panels) obtained in both pp and p -Pb collisions feature broad Gaussian-like peaks versus $\Delta\eta$ whose magnitude decreases with increasing multiplicity. The azimuthal CI projections, by contrast, feature a modulation yielding two maxima: the first, centered at $\Delta\phi = 0$, corresponds to the near-side peak of the correlation functions displayed in Figs. 1 and 2, whereas the second maximum reflects the broad away-side peak of these functions.

The projections of the CD correlators, presented in Figs. 3 and 4 (top panels), feature a somewhat more complex dependence on $\Delta\eta$ and $\Delta\phi$ than those of the CI correlators. In particular, in contrast to the Gaussian-like peaks seen in the CI projections, the CD longitudinal projections exhibit small and narrow dips atop the peak, which is broader than that of the CI projections. The dip is most prominent in the azimuthal projections of the G_2^{CD} correlator and largest in the 70–80% multiplicity class of pp collisions. The width and depth of the dip are manifestly functions of the multiplicity of the collisions and thus appear to feature a system size dependence.

This system size dependence is qualitatively understood as arising, in part, from femtoscopic (HBT) correlations. The CD correlators are computed as the difference between US and LS correlators. The G_2^{LS} correlators, much like the femtoscopic (number) correlation functions measured as a function of the invariant momentum difference of particle pairs, are sensitive to the presence of bosonic interference, and it is well established that the widths of these correlation functions are inversely proportional to the size of the measured system [50]. It is thus expected that G_2^{LS} , measured as function of $\Delta\eta$ or $\Delta\phi$, should also exhibit such a dependence on the system size. This dependence is seen as dips because the LS correlators are subtracted from the US correlators. Additionally, note that the effect is smaller in p -Pb collisions, most likely because of the larger size of the systems formed in these collisions.

VI. SHAPE EVOLUTION WITH MULTIPLICITY

The multiplicity evolution of the shape and strength of the G_2^{CD} and G_2^{CI} correlators measured in pp and p -Pb collisions

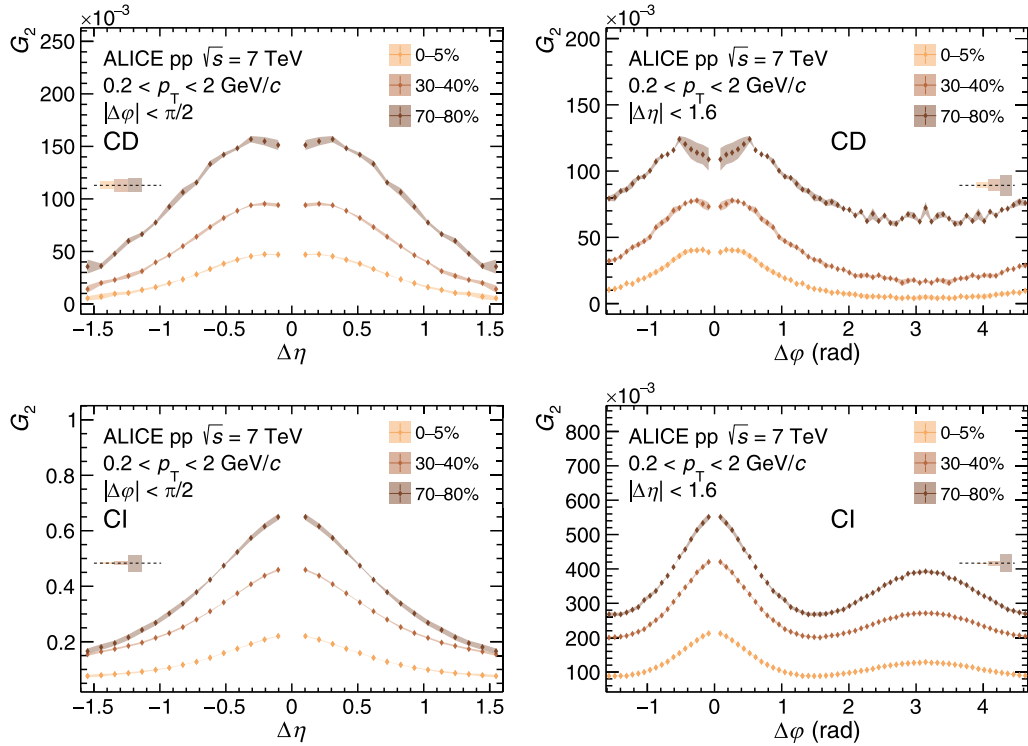


FIG. 3. Longitudinal (left) and azimuthal (right) projections of the two-particle transverse momentum correlations G_2^{CD} (top) and G_2^{CI} (bottom) for selected charged particle multiplicity classes in pp collisions at $\sqrt{s} = 7$ TeV. The correlator values are not shown in the intervals $|\Delta\eta| < 0.1$ and $|\Delta\phi| < 0.09$, which are affected by track merging effects (see text for details). Vertical bars (mostly smaller than the marker size) and shaded bands represent statistical and uncorrelated systematic uncertainties, respectively. Correlated systematic uncertainties are represented as small boxes at the sides of the panels.

is analyzed using a multicomponent model already utilized in Pb-Pb collisions [24] and defined as

$$\begin{aligned}
 F(\Delta\eta, \Delta\phi) = & B + \sum_{n=2}^6 a_n \times \cos(n \Delta\phi) \\
 & + A \times \frac{\gamma_{\Delta\eta}}{2\omega_{\Delta\eta} \Gamma(\frac{1}{\gamma_{\Delta\eta}})} e^{-|\frac{\Delta\eta}{\omega_{\Delta\eta}}|^{\gamma_{\Delta\eta}}} \\
 & \times \frac{\gamma_{\Delta\phi}}{2\omega_{\Delta\phi} \Gamma(\frac{1}{\gamma_{\Delta\phi}})} e^{-|\frac{\Delta\phi}{\omega_{\Delta\phi}}|^{\gamma_{\Delta\phi}}}, \quad (5)
 \end{aligned}$$

where B and a_n are intended to describe the long-range mean correlation strength and the possible azimuthal anisotropies, while the bidimensional generalized Gaussian, defined by the parameters A , $\omega_{\Delta\eta}$, $\omega_{\Delta\phi}$, $\gamma_{\Delta\eta}$, and $\gamma_{\Delta\phi}$, is intended to model the near-side peak.

The main focus of this paper is specifically on measuring the evolution of the azimuthal and longitudinal widths of the prominent near-side peak of the G_2^{CD} and G_2^{CI} correlators, which is quantified in terms of width parameters $\sigma_{\Delta\eta}$ and $\sigma_{\Delta\phi}$ computed according to

$$\sigma_{\Delta\eta(\Delta\phi)} = \sqrt{\frac{\omega_{\Delta\eta(\Delta\phi)}^2 \Gamma(3/\gamma_{\Delta\eta(\Delta\phi)})}{\Gamma(1/\gamma_{\Delta\eta(\Delta\phi)})}}. \quad (6)$$

Bidimensional fits to the measured G_2^{CD} and G_2^{CI} correlators were carried out with the least-squares method, considering only the statistical uncertainties. The central region around

$|\Delta\eta| = 0$ and $|\Delta\phi| = 0$ was excluded from the fit to avoid biases associated with track merging. The excluded region was enlarged, when appropriate, to cover the narrow dip found in the CD correlation functions. The differences between data points and fit functions were examined in detail and found to be negligible relative to the amplitude of the correlation functions except in some areas of the near-side peak tails and close to the excluded patch around $\Delta\eta, \Delta\phi = (0, 0)$, thereby yielding a full fit χ^2/dof in the range 2 to 9. Fits were repeated using systematic uncertainties of the correlation functions to examine the possibility of biases. Widths obtained with these larger uncertainties were within the systematic uncertainties of the nominal values, reported for fits performed with statistical uncertainties, and the χ^2/dof values dropped below unity.

Systematic uncertainties on the extracted widths were assessed using the procedure described in Sec. IV. The largest contributor to these uncertainties is the track selection criteria with values of 4% (2%) and 2% (2%) for the longitudinal and azimuthal widths, respectively, of the G_2^{CD} (G_2^{CI}) correlator in the pp system, and 4% (2%) for both widths in the p -Pb system. Total systematic uncertainties on the widths amount to 5% (2%) and 3% (2%) for the longitudinal and azimuthal widths, respectively, of the G_2^{CD} (G_2^{CI}) correlator in the pp system, and 5% (3%) and 4% (2%) in the p -Pb system.

Figure 5 shows the evolution of the longitudinal and azimuthal widths σ of the G_2^{CD} (top panels) and G_2^{CI} (bottom panels) correlators as a function of the average charged

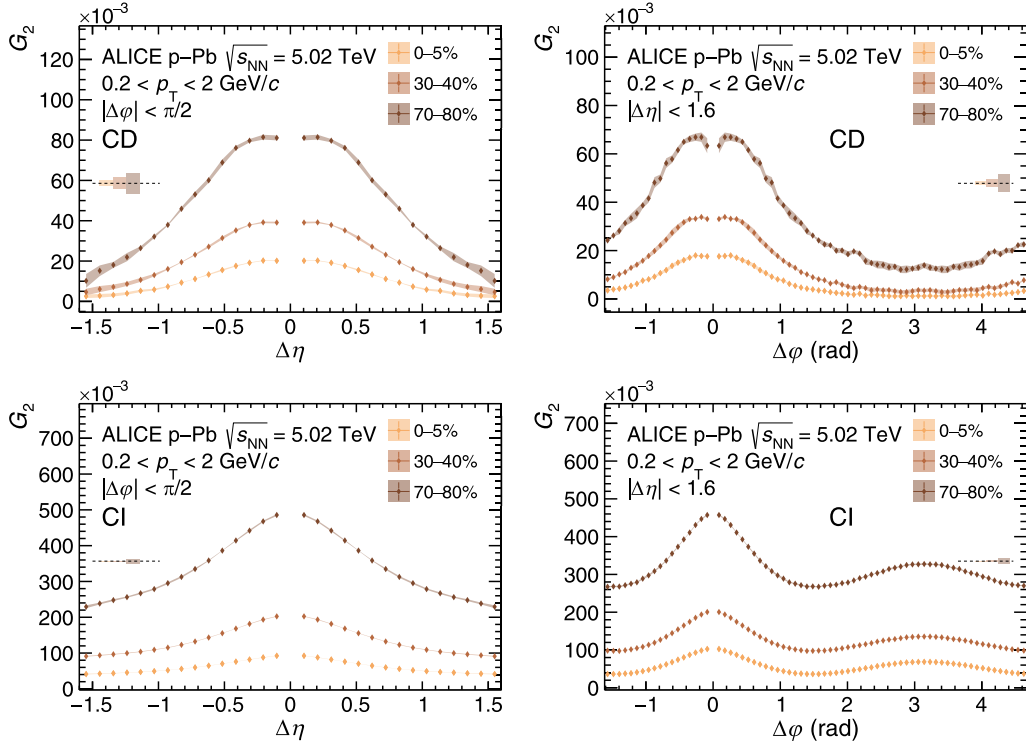


FIG. 4. Longitudinal (left) and azimuthal (right) projections of the two-particle transverse momentum correlations G_2^{CD} (top) and G_2^{CI} (bottom) for selected charged particle multiplicity classes in p -Pb collisions at $\sqrt{s_{\text{NN}}} = 5.02$ TeV. The correlator values are not shown in the intervals $|\Delta\eta| < 0.1$ and $|\Delta\phi| < 0.09$, which are affected by track merging effects (see text for details). Vertical bars (mostly smaller than the marker size) and shaded bands represent statistical and uncorrelated systematic uncertainties, respectively. Correlated systematic uncertainties are represented as small boxes at the sides of the panels.

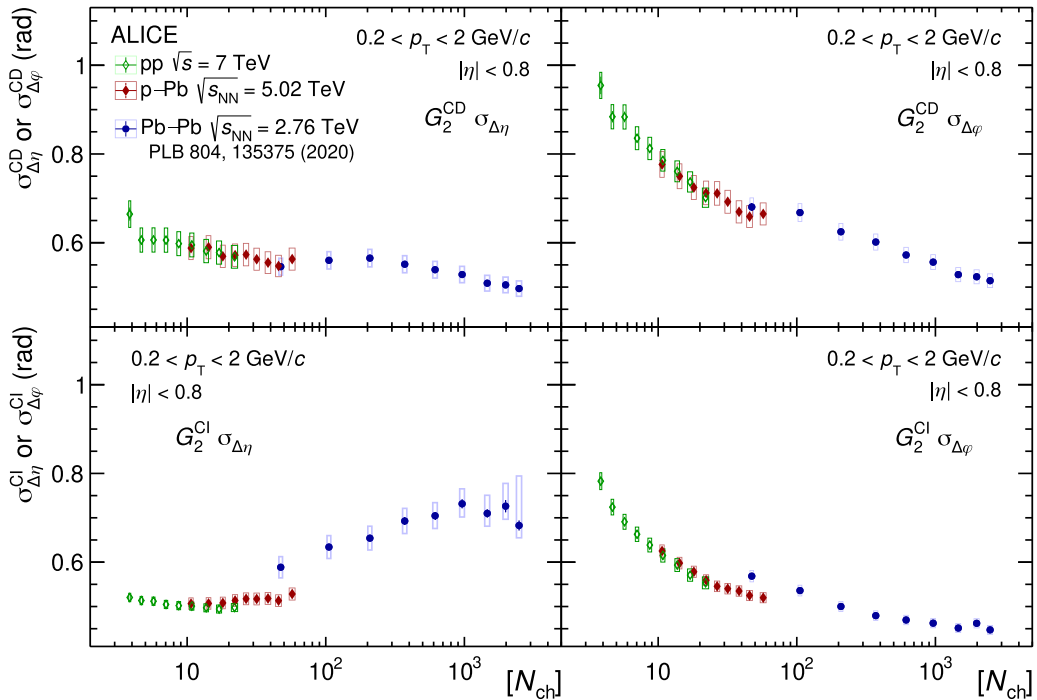


FIG. 5. Evolution with the average charged particle multiplicity of the longitudinal (left) and azimuthal (right) widths of the two-particle transverse momentum differential correlation G_2^{CD} (top row) and G_2^{CI} (bottom row) in pp , p -Pb, and Pb-Pb collisions at $\sqrt{s} = 7$ TeV, $\sqrt{s_{\text{NN}}} = 5.02$ TeV, and $\sqrt{s_{\text{NN}}} = 2.76$ TeV, respectively. Vertical bars (mostly smaller than the marker size) and filled boxes represent statistical and systematic uncertainties, respectively.

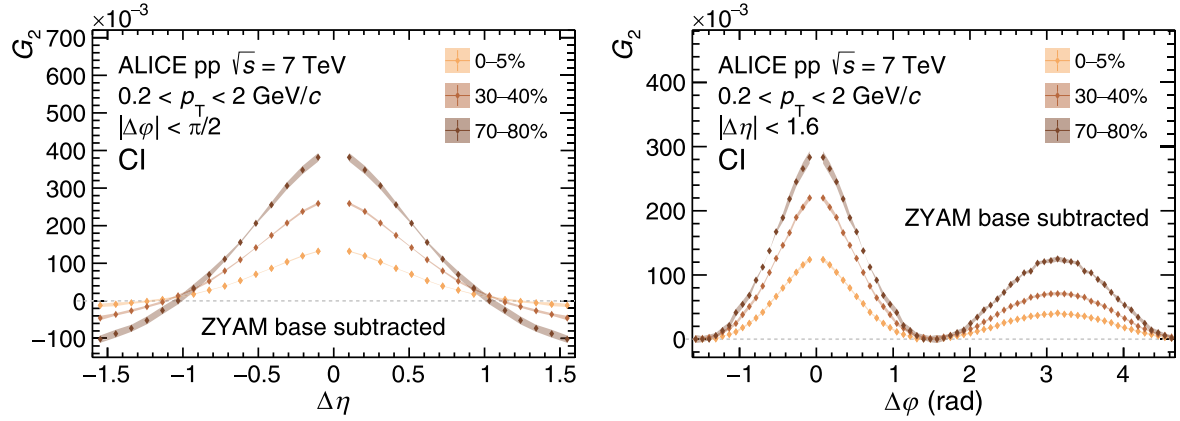


FIG. 6. Longitudinal (left) and azimuthal (right) projections of the two-particle transverse momentum correlation G_2^{CI} for selected charged particle multiplicity classes in pp collisions at $\sqrt{s} = 7$ TeV after subtracting the azimuthal ZYAM base level (see text for details) for each multiplicity class. Vertical bars (mostly smaller than the marker size) and shaded bands represent statistical and uncorrelated systematic uncertainties, respectively.

particle multiplicity $[N_{ch}]$. The G_2^{CD} and G_2^{CI} correlator widths measured in Pb-Pb collisions at $\sqrt{s_{NN}} = 2.76$ TeV by the ALICE Collaboration [24] are also displayed. First focusing on the evolution of the azimuthal and longitudinal widths of the G_2^{CD} correlator with charged particle multiplicity shown in the top panels of Fig. 5, it is observed that this correlator exhibits a strong azimuthal narrowing with increasing $[N_{ch}]$ in both pp and p -Pb collisions and a somewhat weaker narrowing trend in the longitudinal direction. A qualitatively similar narrowing, first reported in Ref. [24], is also observed in Pb-Pb interactions across a broad range of collision multiplicities in both the longitudinal and azimuthal directions. Overall, both the longitudinal and azimuthal widths of the near-side peak in the G_2^{CD} correlator show a smooth narrowing trend with increasing multiplicity across the three different collision systems here considered.

Shifting the focus to the bottom panels of Fig. 5, it is readily noticed that the G_2^{CI} correlator features different evolutions with $[N_{ch}]$ in the azimuthal and the longitudinal directions. A strong narrowing with increasing $[N_{ch}]$ is observed for the azimuthal width, $\sigma_{\Delta\phi}$, in pp and p -Pb collisions, as well as in Pb-Pb collisions [24]. The magnitude and the evolution with $[N_{ch}]$ of the azimuthal widths measured in pp and p -Pb collisions are consistent between each other. In contrast, the width measured in the lowest Pb-Pb multiplicity class (most peripheral collisions), exceeds the widths observed at similar multiplicity in p -Pb collisions by $\approx 8\%$ thereby indicating a difference between the correlations established in p -Pb and Pb-Pb collisions with similar charged particle multiplicity.

The $[N_{ch}]$ evolution of the longitudinal width of the G_2^{CI} correlator is different for the three collision systems and contrasts markedly from the trend measured for the azimuthal width $\sigma_{\Delta\phi}$. In pp collisions, the width exhibits a trend consistent with a very modest narrowing with increasing $[N_{ch}]$ whereas, in p -Pb collisions, the data suggests a weak increase with $[N_{ch}]$. It is also found that at equal values of $[N_{ch}]$ the longitudinal widths measured in p -Pb are also somewhat larger than those observed in pp collisions even though they

are compatible within uncertainties. The increasing trend seen in p -Pb is difficult to precisely assess given the size of the systematic uncertainties relative to the very modest increase of the width. It is rather clear, nonetheless, that it does not match the rapid and large increase observed in Pb-Pb collisions. Indeed, at $[N_{ch}] \approx 50$, the longitudinal width observed in Pb-Pb exceeds that measured in p -Pb collisions by $\approx 13\%$. The slope of the increasing trend of $\sigma_{\Delta\eta}$ in Pb-Pb collisions far exceeds that seen in p -Pb. By extrapolating the trend observed in Pb-Pb to small $[N_{ch}]$, the obtained $\sigma_{\Delta\eta}$ values match those measured in pp collisions but it is rather clear that the broadening observed in Pb-Pb collisions stands in stark contrast to the evolution observed in the smaller systems. Overall, the current measurements indicate that, while the azimuthal widths of the CD and CI correlators in pp and p -Pb collisions show a trend with multiplicity compatible with that found in the larger Pb-Pb system, the evolution of the longitudinal width of the G_2^{CI} correlator is rather different in small and large systems.

It is of interest to contrast the results of the bidimensional fit procedure used in this work with those obtained with the zero yield at minimum (ZYAM) method [51] widely used in the analysis of azimuthal correlation functions. The difficulty with ZYAM is that if the peaks are wide in $\Delta\phi$, the gap between the near-side and away-side peaks gets “filled up” in the projection. In particular, if the ZYAM method is indiscriminately applied to correlation functions with a strong dependence on the longitudinal particle pair separation, $\Delta\eta$, significant biases may occur in the evaluation of the amplitudes and widths of such correlations and their dependence on the global event observables.

As an illustration, the right panel of Fig. 6 shows the azimuthal projections of the G_2^{CI} correlator for three selected multiplicity classes, after applying the ZYAM procedure to remove “uncorrelated backgrounds,” i. e., by uniformly subtracting a constant value corresponding to the minimum yield value, hereafter called ZYAM base level. The widths extracted based on these projections are approximately the same for the different multiplicity classes considered, thereby leading to

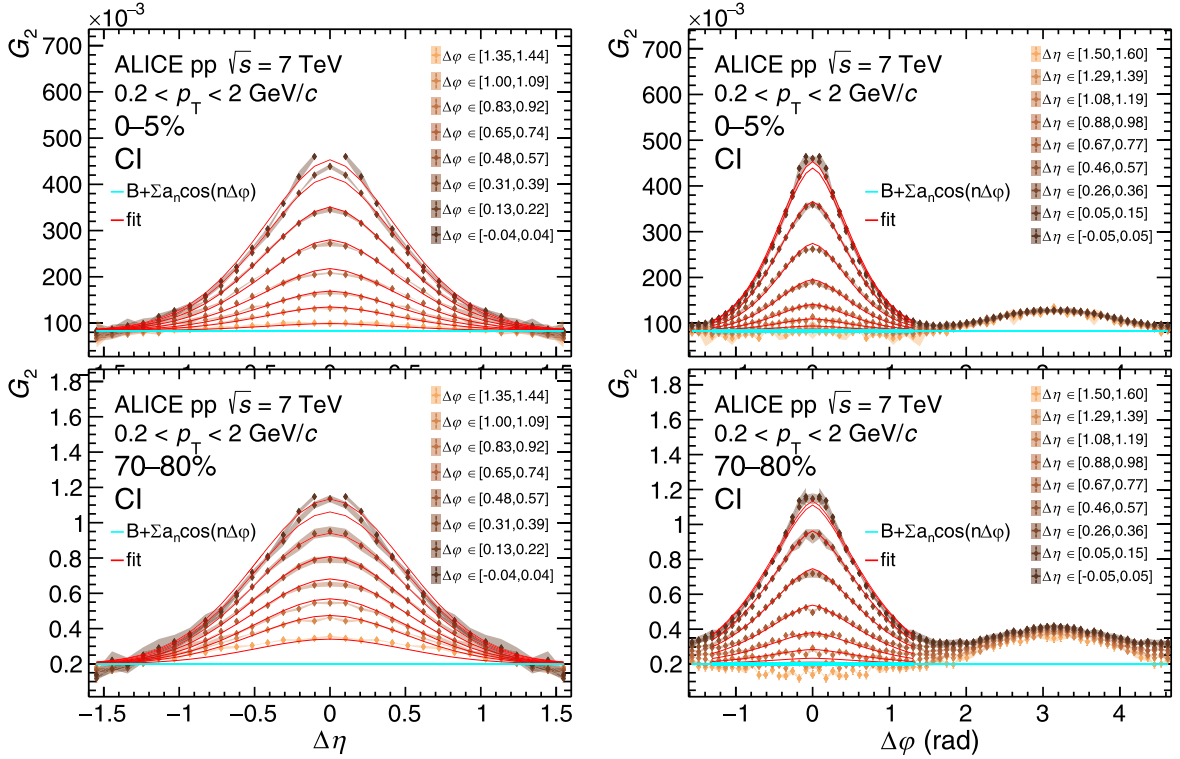


FIG. 7. Longitudinal projections of slices of one azimuthal bin (left) and azimuthal projections of slices of one longitudinal bin (right), for selected bins of the two-particle transverse momentum correlation G_2^{CI} and its bidimensional fit using Eq. (5) for the 0–5% (top) and 70–80% (bottom) charged particle multiplicity classes in pp collisions at $\sqrt{s} = 7$ TeV. Vertical bars (mostly smaller than the marker size) and shaded bands represent statistical and uncorrelated systematic uncertainties, respectively.

the conclusion that the width of these correlation functions is independent of the multiplicity class. In the left panel of Fig. 6, the near-side longitudinal projections of the G_2^{CI} correlator are shown after subtraction of the ZYAM base level. Parts of the longitudinal projections lie significantly below zero, with values that depend on the multiplicity class. The notion of zero yield at minimum is thus rather poorly defined in this context given that the minimum of the longitudinal correlations (within the measurement acceptance) significantly deviates from the ZYAM base level and is a monotonic function of the multiplicity class. The application of the ZYAM method consequently does not enable a simultaneous consistent extraction of the azimuthal and longitudinal widths of the G_2^{CI} correlators measured in this work.

By contrast, the fit method used in this work parametrizes the correlation functions with a bidimensional generalized Gaussian model, Eq. (5), with independent parameters along the $\Delta\eta$ and $\Delta\phi$ directions, thereby enabling a more accurate description of the shape of the G_2^{CI} correlator and its dependence on the multiplicity $[N_{ch}]$. For illustrative purposes, Fig. 7 compares several projections of the two-dimensional fit functions (red lines) and the data (solid diamonds) for the CI correlators in the 0–5% and 70–80% multiplicity classes of pp collisions. Projections onto $\Delta\eta$ (left panels) are shown for selected ranges of $\Delta\phi$ pair separation, and, conversely, projections onto $\Delta\phi$ (right panels) are displayed for selected ranges of $\Delta\eta$ pair separation. The cyan lines represent the baseline B plus the anisotropic modulations given by the

coefficients a_n in the fit function, extended to the whole azimuthal range in the case of the azimuthal projections, in which the thicker line section represents the azimuthal portion considered for the bidimensional fit. The two-dimensional fits provide good descriptions of most of the azimuthal slices, shown in the left panels, (i. e., irrespective of the multiplicity class and $\Delta\phi$ range) as well as good match on most of the longitudinal slices, shown in the right panels. Deviations of the model from data are observed at large longitudinal relative separation, visible for slices at large $\Delta\eta$, and in the proximity of $\Delta\eta, \Delta\phi = (0, 0)$. The two-dimensional generalized Gaussian model used in this work thus provides a reliable, robust, and self-consistent description of the G_2^{CI} correlator measurements. The azimuthal and longitudinal widths extracted from this model thus do not suffer from the biased and inconsistent behavior obtained with the ZYAM method. The right panels of Fig. 7, displaying the $\Delta\phi$ projections of G_2^{CI} , provide a simple explanation of the bias encountered with the basic ZYAM method. The shape and strength of the away side, $\pi/2 \leq \Delta\phi < 3\pi/2$, are essentially independent of the $\Delta\eta$ range considered whereas the near side, $|\Delta\phi| < \pi/2$, is strongly dependent on $\Delta\eta$. The ZYAM values of these $\Delta\phi$ projections therefore depend on $\Delta\eta$ and the multiplicity classes. This thus results in inconsistent extractions of the longitudinal and azimuthal widths of the correlator if the basic ZYAM method is used. Such issues are clearly avoided with the two-dimensional generalized Gaussian fit method utilized in this work.

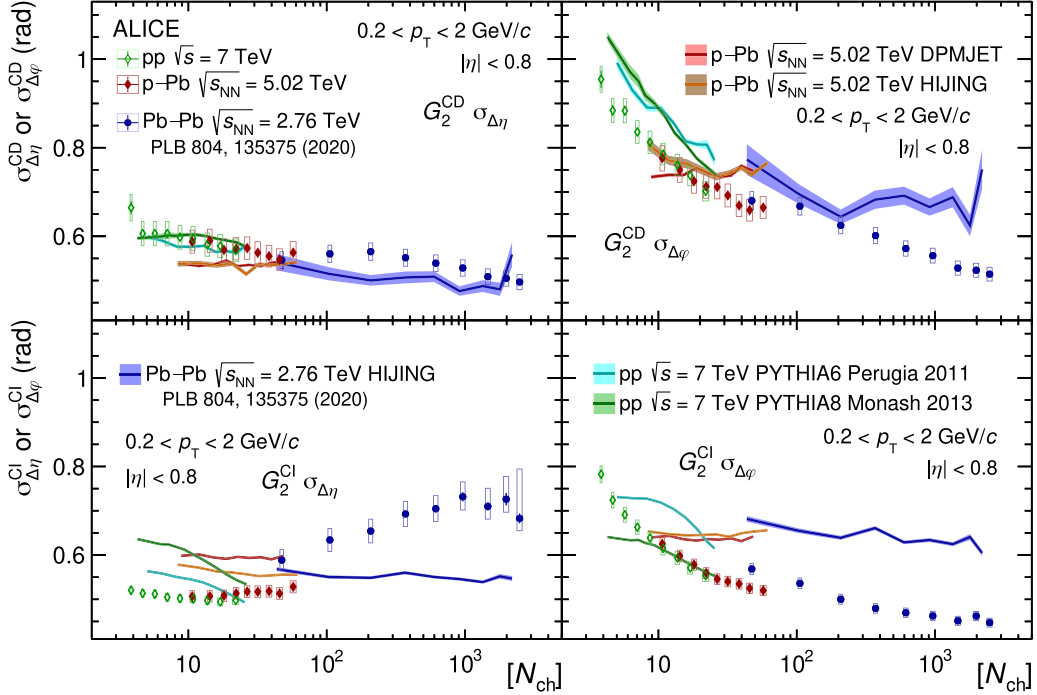


FIG. 8. Evolution with the average charged particle multiplicity of the longitudinal (left) and azimuthal (right) widths of the two-particle transverse momentum correlations G_2^{CD} (top row) and G_2^{CI} (bottom row) in pp , p -Pb, and Pb-Pb collisions at $\sqrt{s} = 7$ TeV, $\sqrt{s_{\text{NN}}} = 5.02$ TeV, and $\sqrt{s_{\text{NN}}} = 2.76$ TeV, respectively, compared to models. Statistical and systematic uncertainties of the data points are shown as vertical bars (mostly smaller than the marker size) and filled boxes, respectively, while the thickness of the shaded bands represents statistical uncertainties of the models. The data points and the results of HIJING simulations for Pb-Pb collisions are taken from Ref. [24].

VII. COMPARISON WITH RESULTS FROM EVENT GENERATORS

A number of event generators have had great successes in quantitatively reproducing the many features and properties of particle production in pp , p -Pb, and Pb-Pb collisions [52–58]. It is thus legitimate to consider whether such production models can also match the magnitude and the evolution with $[N_{\text{ch}}]$ of the near-side peak widths reported in Fig. 5. Comparisons of calculations of the two-particle number correlator $R_2(\Delta\eta, \Delta\varphi)$ and the two-particle transverse momentum correlator $P_2(\Delta\eta, \Delta\varphi)$ performed with the AMPT, EPOS, and URQMD models [59] with data reported by the ALICE Collaboration [32] show these three event generators are considerably challenged by the measurements. In particular, since these models do not fully implement charge and baryon number conservation, they cannot reproduce the salient features of the measured R_2^{CD} and P_2^{CD} correlators, while they qualitatively reproduce some but not all facets of the measured R_2^{CI} and P_2^{CI} correlation functions.

The discussion in this section is limited to four well established models: PYTHIA 6 [46] (Perugia default tune [47]) and PYTHIA 8 [60] (Monash tune, with color reconnection [61]) for comparison with pp data, DPMJET [48] for comparison with p -Pb data, and HIJING [62] for comparison with both p -Pb and Pb-Pb data. PYTHIA and DPMJET are known to well reproduce measurements of differential cross section in pp collisions and, although HIJING does not include a modeling of the collective behavior observed in Pb-Pb, it is here used as a

baseline reference for the discussion of trends as a function of multiplicity in that system. Simulated data sets produced with these four event generators are analyzed, at generator level, with identical event and charged particle selection criteria and multiplicity classes as the data. This allows one to obtain the $G_2^{\text{CD}}(\Delta\eta, \Delta\varphi)$ and $G_2^{\text{CI}}(\Delta\eta, \Delta\varphi)$ correlation functions, which are then fitted with Eq. (5). The width parameters obtained from the fits to the simulated correlators are compared to the measured ones in Fig. 8. The data from Pb-Pb collisions and the results of simulations with HIJING are taken from Ref. [24].

In the case of the charge dependent correlator G_2^{CD} shown in the top panels of Fig. 8, the measured magnitude and multiplicity dependence of the longitudinal width of the near-side peak, $\sigma_{\Delta\eta}^{\text{CD}}$, are described within uncertainties by both PYTHIA 6 and PYTHIA 8 simulations. The two PYTHIA tunes also qualitatively reproduce the observed narrowing trend of the azimuthal width of G_2^{CD} as a function of $[N_{\text{ch}}]$ even though they overestimate the magnitude of $\sigma_{\Delta\varphi}$. By contrast, although DPMJET and HIJING qualitatively reproduce the magnitudes of the longitudinal and azimuthal widths of the G_2^{CD} correlator, they have rather limited success in describing the evolution with multiplicity of the azimuthal widths observed in p -Pb and Pb-Pb collisions.

In the bottom panels of Fig. 8, the measured evolution of the G_2^{CI} correlator widths, $\sigma_{\Delta\eta}^{\text{CI}}$ and $\sigma_{\Delta\varphi}^{\text{CI}}$, with multiplicity is compared to model predictions. PYTHIA 8 describes well the measured azimuthal widths $\sigma_{\Delta\varphi}$ for large multiplicities, but it underestimates them for low multiplicity pp collisions ($[N_{\text{ch}}] < 10$). Instead PYTHIA 6 grossly overestimates the

width and misses the observed trend as a function of $[N_{\text{ch}}]$. Neither of the two PYTHIA versions successfully reproduces the $[N_{\text{ch}}]$ evolution of $\sigma_{\Delta\eta}^{\text{CI}}$, although PYTHIA 6 quantitatively matches the width observed in the highest pp multiplicity class. Similarly, predictions by both DPMJET and HIJING clearly overestimate the longitudinal and azimuthal widths measured in p -Pb collisions. Although HIJING manages to approximately match the longitudinal width observed at lowest multiplicity in Pb-Pb collisions, it systematically underpredicts the $\sigma_{\Delta\eta}$ values measured in higher Pb-Pb multiplicity classes and thus fails to match the broadening trend of $\sigma_{\Delta\eta}^{\text{CI}}$ vs. $[N_{\text{ch}}]$. Overall, the models considered for the comparison match the evolution of the longitudinal and azimuthal widths of G_2^{CD} the closest while doing rather poorly for the evolution of the widths of G_2^{CI} . This suggests that their ability to describe charge conserving processes is decent but that, globally, some new features are needed to properly match the evolution of the widths of G_2^{CI} .

VIII. DISCUSSION

The inspection of the evolution of the G_2^{CD} and G_2^{CI} correlators with the multiplicity of charged particles produced in the collision suggests that two or more competing mechanisms may be at play in pp , p -Pb, and Pb-Pb collisions: while the near side peak of G_2^{CD} shows narrowing trends with increasing $[N_{\text{ch}}]$ in these systems, G_2^{CI} exhibits mixed trends in the longitudinal dimension, a strong broadening in Pb-Pb, minor broadening in p -Pb, and modest narrowing in pp collisions.

A narrowing of the near-side peak of two-particle correlators has been observed for R_2^{CD} and P_2^{CD} differential correlators of low- p_{T} particles measured in Pb-Pb collisions at $\sqrt{s_{\text{NN}}} = 2.76$ TeV [32], for balance functions of charged particles and identified hadrons in pp , p -Pb, and Pb-Pb collisions at 7, 5.02, and 2.76 TeV, respectively [31,63,64], as well as in Au-Au collisions at RHIC energies [65–67]. Measurements in large collision systems show that the average transverse momentum of produced particles, $\langle p_{\text{T}} \rangle$, rises monotonically with increasing multiplicity in Au-Au and Pb-Pb collisions and saturates in most central collisions. Similarly, blast-wave model fits of p_{T} spectra measured as a function of increasing collision centrality in these systems indicate that the radial flow velocity increases with increasing multiplicity of produced particles [68,69]. Moreover, theoretical studies of the evolution of the narrowing of charge balance functions, B_{ch} , in Au-Au collisions based on the blast-wave model are found to require strong radial flow to match the progressive narrowing of the near-side peak of these correlation functions [70]. Similar narrowing effects and large radial flow are also seen in hydrodynamics calculations [71].

Given that G_2 shares the same correlation kernel as the R_2 , P_2 , and B_{ch} correlators, the progressive narrowing of its near-side peak with increasing values of $[N_{\text{ch}}]$ in Pb-Pb collisions can be interpreted as resulting from the increasing radial flow velocity. An increase of $\langle p_{\text{T}} \rangle$ with increasing multiplicity is also observed in pp and p -Pb collisions [26]. However, it is still an open question whether this increase results from the production of a radially flowing medium also in these small

collision systems. In any case, it is expected that an increase in $\langle p_{\text{T}} \rangle$ should also produce a kinematic focusing of correlated particles, resulting in a narrowing of the correlation peaks. A modest narrowing of the R_2^{CD} and P_2^{CD} correlation functions has already been reported in p -Pb collisions [32] and is, with this work, also established for the azimuthal widths of G_2^{CD} and G_2^{CI} correlators observed in the pp and p -Pb systems. It is then plausible to postulate that the azimuthal narrowing of the correlators results from collective radial flow in these smaller systems.

The details of the evolution of the widths $\sigma_{\Delta\eta}^{\text{CD}}$ and $\sigma_{\Delta\eta}^{\text{CI}}$ with $[N_{\text{ch}}]$ are consequently of particular interest. As already suggested, both these widths exhibit a monotonic narrowing with increasing $[N_{\text{ch}}]$ in all three systems studied. However, their evolution is not continuous between systems. Indeed, at equal particle production $[N_{\text{ch}}]$, the width of these correlators in p -Pb collisions is similar, within uncertainties, to that observed in pp collisions. Additionally, although measurements in p -Pb and Pb-Pb collisions have a limited overlap in $[N_{\text{ch}}]$, the $\sigma_{\Delta\eta}^{\text{CI}}$ widths measured in Pb-Pb are approximately 8% larger than those observed in p -Pb. These differences can qualitatively be interpreted as resulting from the size of the systems considered. The lowest multiplicity measurement of G_2 in Pb-Pb collisions shown in Fig. 5 corresponds to the 70–80% collision centrality class. In this range, the average number of nucleons participating in the Pb-Pb collision amounts to approximately 15 [72] and should far exceed the number of participants involved in a typical p -Pb collision. Although estimates of the number of participant nucleons in p -Pb collisions are less precise than in the Pb-Pb case, it can be reasonably expected that at a given value of $[N_{\text{ch}}]$ p -Pb collisions involve on average more participants than pp collisions. At a given value of $[N_{\text{ch}}]$, p -Pb collisions (Pb-Pb collisions) are thus expected to consist of a lower number of contributors from hard scatterings than those produced in pp (p -Pb) collisions. It is then reasonable to expect that these correlators in different collision systems have slightly different widths at equal $[N_{\text{ch}}]$ value. In any case, comprehensive models of particle production in small and large systems should account for these small differences, and the evolution of the azimuthal width of G_2^{CD} thus constitutes a stringent test of such models.

The three systems exhibit a rather different evolution of the longitudinal width $\sigma_{\Delta\eta}^{\text{CI}}$ with increasing $[N_{\text{ch}}]$. Whereas $\sigma_{\Delta\eta}^{\text{CI}}$ increases from 0.59 to a maximum value of 0.73 (24%) with increasing $[N_{\text{ch}}]$ in Pb-Pb collisions, it decreases by about 5% in pp while rising by approximately the same amount in p -Pb collisions. A broadening of the longitudinal width of the near-side peak in the G_2^{CI} correlator was also observed in Au-Au collisions at RHIC [73] and was predicted to occur as a result of viscous forces in collision systems producing a long lived QGP phase [21]. In this context, the medium formed in the collision is modeled as a fluid in quasiequilibrium. Fluid cells are accelerated by local pressure gradients and do not, *ab initio*, have equal transverse velocities. Viscous interactions between cells are then expected to slow down fast moving cells and accelerate cells with smaller transverse velocity. The resulting momentum transfers are then expected to induce “long range” longitudinal correlations between cells and the

particles they emit, thereby producing broadened two-particle correlation functions relative to systems that do not undergo viscous forces.

The Pb-Pb system clearly manifests the behavior expected from a long lived viscous fluid: the average transverse momentum monotonically increases with increasing multiplicity of produced particles, the width $\sigma_{\Delta\varphi}^{\text{CD}}$ monotonically decreases, whereas the width $\sigma_{\Delta\eta}^{\text{CI}}$ increases with increasing multiplicity and is consistent with a fluid characterized by a small value of η/s [24,25].

The behavior and nature of the pp and p -Pb systems are much less clear. While both collisions systems exhibit the $\sigma_{\Delta\varphi}^{\text{CD}}$ narrowing expected from a fluid undergoing radial flow and anisotropic particle emission in the transverse plane, the width $\sigma_{\Delta\eta}^{\text{CI}}$ decreases with increasing multiplicity in pp collisions while exhibiting a very modest increase in p -Pb collisions. No conclusion can therefore be drawn on the possible establishment of a collective behavior in pp collisions, while the results from p -Pb collisions provide only a suggestive indication, limited by the magnitude of systematic uncertainties, for the presence of viscous effects. The interpretation of trends observed in these two collision systems is further complicated by the presence of competing effects resulting from radial flow. The longitudinal widths $\sigma_{\Delta\eta}^{\text{CD}}$ in pp and p -Pb collisions exhibit a narrowing trend with increasing $[N_{\text{ch}}]$ that should be matched, in the absence of viscous effects, by a similar behavior for $\sigma_{\Delta\eta}^{\text{CI}}$. Such small narrowing effect may then compete with and partly mask the viscous broadening that would otherwise occur in such small systems. It should also be considered that possible viscous forces would need time to propagate correlations in the longitudinal direction. Thus, the longitudinal broadening of G_2 shall depend both on the magnitude of the shear viscosity (per unit entropy) and the lifetime of the fluid. If the fluidlike system produced is too small or too short lived, there may not be enough time for viscous forces to equalize the transverse velocity differences between cells and, even though a fluid-like system may be produced in pp or p -Pb collisions, it may not live long enough to yield a significant broadening of the G_2^{CI} correlator. Competing effects associated with kinematic focusing may then hinder observations of viscous broadening.

Alternatively, it is also possible that a quasiequilibrated fluid description does not hold for the system produced in pp and p -Pb collisions. Appealing to more traditional models to interpret the data is then needed. However, as already noted, while PYTHIA 6 manages to qualitatively reproduce the narrowing of the CD correlator, it poorly describes the measurements for the CI correlator. Similarly, PYTHIA 8 (Monash tune, with color reconnection) qualitatively reproduces the azimuthal widths but introduces too much narrowing in the longitudinal dimension of the CI correlator.

IX. CONCLUSIONS

The two-particle transverse momentum differential correlators G_2^{CI} and G_2^{CD} were measured in pp collisions at $\sqrt{s} = 7$ TeV and in p -Pb collisions at $\sqrt{s_{\text{NN}}} = 5.02$ TeV as a function of the charged hadron multiplicity measured in the selected acceptance, $[N_{\text{ch}}]$. Both correlators feature

prominent near-side peaks. The amplitude of these peaks decreases monotonically with increasing charged hadron multiplicity, N_{ch} , in both collision systems, but their widths exhibit mixed behaviors.

The near-side peak of the G_2^{CI} and G_2^{CD} correlators exhibits strong azimuthal narrowing trends with increasing N_{ch} , in pp and p -Pb collisions, that qualitatively match the width evolution with collision centrality formerly observed in the Pb-Pb system. The G_2^{CD} near-side peak also features a longitudinal narrowing albeit weaker than that observed in the azimuthal direction. The narrowing trends observed in pp collisions are qualitatively reproduced by PYTHIA, even with PYTHIA 6 Perugia tune, thereby indicating that the evolution of the two correlators is well accounted for by this model, i. e., without the need to invoke a collective behavior. However, the multiplicity dependence measured in p -Pb collisions is not described by DPMJET.

The longitudinal width, $\sigma_{\Delta\eta}^{\text{CI}}$, of the G_2^{CI} correlator in pp and p -Pb collisions is not varying with multiplicity, within uncertainties, at variance with the case of Pb-Pb collisions. The lack of a clear dependence on multiplicity of the widths in pp and p -Pb collisions provides no evidence of an increase of $\sigma_{\Delta\eta}^{\text{CI}}$ within uncertainties. It is possible that, if fluidlike systems are produced in p -Pb collisions, they are too short lived for viscous forces to have a sizable impact on the width of the correlator. Further studies of the p -Pb system are thus required to fully elucidate its behavior.

ACKNOWLEDGMENTS

The ALICE Collaboration would like to thank all its engineers and technicians for their invaluable contributions to the construction of the experiment and the CERN accelerator teams for the outstanding performance of the LHC complex. The ALICE Collaboration gratefully acknowledges the resources and support provided by all Grid centres and the Worldwide LHC Computing Grid (WLCG) Collaboration. The ALICE Collaboration acknowledges the following funding agencies for their support in building and running the ALICE detector: A. I. Alikhanyan National Science Laboratory (Yerevan Physics Institute) Foundation (ANSL), State Committee of Science and World Federation of Scientists (WFS), Armenia; Austrian Academy of Sciences, Austrian Science Fund (FWF) [M 2467-N36], and Nationalstiftung für Forschung, Technologie und Entwicklung, Austria; Ministry of Communications and High Technologies, National Nuclear Research Center, Azerbaijan; Conselho Nacional de Desenvolvimento Científico e Tecnológico (CNPq), Financiadora de Estudos e Projetos (Finep), Fundação de Amparo à Pesquisa do Estado de São Paulo (FAPESP), and Universidade Federal do Rio Grande do Sul (UFRGS), Brazil; Bulgarian Ministry of Education and Science, within the National Roadmap for Research Infrastructures 2020–2027 (object CERN), Bulgaria; Ministry of Education of China (MOEC), Ministry of Science & Technology of China (MSTC), and National Natural Science Foundation of China (NSFC), China; Ministry of Science and Education and Croatian Science Foundation, Croatia; Centro de Aplicaciones Tecnológicas y Desarrollo Nuclear (CEADEN), Cubaenergía, Cuba; Ministry of Education,

Youth and Sports of the Czech Republic, Czech Republic; The Danish Council for Independent Research–Natural Sciences, the VILLUM FONDEN, and Danish National Research Foundation (DNRF), Denmark; Helsinki Institute of Physics (HIP), Finland; Commissariat à l’Energie Atomique (CEA) and Institut National de Physique Nucléaire et de Physique des Particules (IN2P3) and Centre National de la Recherche Scientifique (CNRS), France; Bundesministerium für Bildung und Forschung (BMBF) and GSI Helmholtzzentrum für Schwerionenforschung GmbH, Germany; General Secretariat for Research and Technology, Ministry of Education, Research and Religions, Greece; National Research, Development and Innovation Office, Hungary; Department of Atomic Energy Government of India (DAE), Department of Science and Technology, Government of India (DST), University Grants Commission, Government of India (UGC), and Council of Scientific and Industrial Research (CSIR), India; National Research and Innovation Agency–BRIN, Indonesia; Istituto Nazionale di Fisica Nucleare (INFN), Italy; Japanese Ministry of Education, Culture, Sports, Science and Technology (MEXT) and Japan Society for the Promotion of Science (JSPS) KAKENHI, Japan; Consejo Nacional de Ciencia (CONACYT) y Tecnología, through Fondo de Cooperación Internacional en Ciencia y Tecnología (FONCICYT) and Dirección General de Asuntos del Personal Académico (DGAPA), Mexico; Nederlandse Organisatie voor Wetenschappelijk Onderzoek (NWO), Netherlands; The Research Council of Norway, Norway; Commission on Science and Technology for Sustainable Development in the South (COMSATS), Pakistan; Pontificia Universidad Católica del

Perú, Peru; Ministry of Education and Science, National Science Centre and WUT ID-UB, Poland; Korea Institute of Science and Technology Information and National Research Foundation of Korea (NRF), Republic of Korea; Ministry of Education and Scientific Research, Institute of Atomic Physics, Ministry of Research and Innovation and Institute of Atomic Physics, and University Politehnica of Bucharest, Romania; Ministry of Education, Science, Research and Sport of the Slovak Republic, Slovakia; National Research Foundation of South Africa, South Africa; Swedish Research Council (VR) and Knut & Alice Wallenberg Foundation (KAW), Sweden; European Organization for Nuclear Research, Switzerland; Suranaree University of Technology (SUT), National Science and Technology Development Agency (NSTDA), Thailand Science Research and Innovation (TSRI), and National Science, Research and Innovation Fund (NSRF), Thailand; Turkish Energy, Nuclear and Mineral Research Agency (TENMAK), Turkey; National Academy of Sciences of Ukraine, Ukraine; Science and Technology Facilities Council (STFC), United Kingdom; National Science Foundation of the United States of America (NSF) and United States Department of Energy, Office of Nuclear Physics (DOE NP), United States of America. In addition, individual groups or members have received support from Marie Skłodowska Curie, European Research Council, Strong 2020–Horizon 2020 (Grants No. 950692, No. 824093, No. 896850), European Union; Academy of Finland (Center of Excellence in Quark Matter) (Grants No. 346327, No. 346328), Finland; Programa de Apoyos para la Superación del Personal Académico, UNAM, Mexico.

-
- [1] J. Adams *et al.* (STAR Collaboration), Experimental and theoretical challenges in the search for the quark gluon plasma: The STAR Collaboration’s critical assessment of the evidence from RHIC collisions, *Nucl. Phys. A* **757**, 102 (2005).
- [2] K. Adcox *et al.* (PHENIX Collaboration), Formation of dense partonic matter in relativistic nucleus-nucleus collisions at RHIC: Experimental evaluation by the PHENIX Collaboration, *Nucl. Phys. A* **757**, 184 (2005).
- [3] I. Arsene *et al.* (BRAHMS Collaboration), Quark gluon plasma and color glass condensate at RHIC? The perspective from the BRAHMS experiment, *Nucl. Phys. A* **757**, 1 (2005).
- [4] B. B. Back *et al.* (PHOBOS Collaboration), The PHOBOS perspective on discoveries at RHIC, *Nucl. Phys. A* **757**, 28 (2005).
- [5] K. Aamodt *et al.* (ALICE Collaboration), Elliptic Flow of Charged Particles in Pb-Pb Collisions at 2.76 TeV, *Phys. Rev. Lett.* **105**, 252302 (2010).
- [6] B. B. Abelev *et al.* (ALICE Collaboration), Centrality, rapidity and transverse momentum dependence of J/ψ suppression in Pb-Pb collisions at $\sqrt{s_{NN}}=2.76$ TeV, *Phys. Lett. B* **734**, 314 (2014).
- [7] J. Adam *et al.* (ALICE Collaboration), Measurement of jet suppression in central Pb-Pb collisions at $\sqrt{s_{NN}} = 2.76$ TeV, *Phys. Lett. B* **746**, 1 (2015).
- [8] J. Adam *et al.* (ALICE Collaboration), J/ψ suppression at forward rapidity in Pb-Pb collisions at $\sqrt{s_{NN}} = 5.02$ TeV, *Phys. Lett. B* **766**, 212 (2017).
- [9] A. M. Sirunyan *et al.* (CMS Collaboration), Measurement of prompt and nonprompt charmonium suppression in Pb-Pb collisions at 5.02 TeV, *Eur. Phys. J. C* **78**, 509 (2018).
- [10] A. M. Sirunyan *et al.* (CMS Collaboration), Measurement of nuclear modification factors of $\Upsilon(1S)$, $\Upsilon(2S)$, and $\Upsilon(3S)$ mesons in Pb-Pb collisions at $\sqrt{s_{NN}} = 5.02$ TeV, *Phys. Lett. B* **790**, 270 (2019).
- [11] S. Acharya *et al.* (ALICE Collaboration), Production of charged pions, kaons, and (anti-)protons in Pb-Pb and inelastic pp collisions at $\sqrt{s_{NN}} = 5.02$ TeV, *Phys. Rev. C* **101**, 044907 (2020).
- [12] H. Song, S. A. Bass, U. Heinz, T. Hirano, and C. Shen, 200A GeV Au+Au Collisions Serve a Nearly Perfect Quark-Gluon Liquid, *Phys. Rev. Lett.* **106**, 192301 (2011); **109**, 139904(E) (2012).
- [13] Z. Qiu, C. Shen, and U. Heinz, Hydrodynamic elliptic and triangular flow in Pb-Pb collisions at $\sqrt{s} = 2.76A$ TeV, *Phys. Lett. B* **707**, 151 (2012).
- [14] H. Song, Hydrodynamic modeling and the QGP shear viscosity, *Eur. Phys. J. A* **48**, 163 (2012).
- [15] C. Gale, S. Jeon, and B. Schenke, Hydrodynamic modeling of heavy-ion collisions, *Int. J. Mod. Phys. A* **28**, 1340011 (2013).
- [16] U. Heinz and R. Snellings, Collective flow and viscosity in relativistic heavy-ion collisions, *Annu. Rev. Nucl. Part. Sci.* **63**, 123 (2013).
- [17] J. E. Bernhard, J. S. Moreland, and S. A. Bass, Bayesian estimation of the specific shear and bulk viscosity of quark-gluon plasma, *Nat. Phys.* **15**, 1113 (2019).

- [18] S. Acharya *et al.* (ALICE Collaboration), Multiharmonic Correlations of Different Flow Amplitudes in Pb-Pb Collisions at $\sqrt{s_{NN}} = 2.76$ TeV, *Phys. Rev. Lett.* **127**, 092302 (2021).
- [19] J. Adam *et al.* (ALICE Collaboration), Correlated Event-by-Event Fluctuations of Flow Harmonics in Pb-Pb Collisions at $\sqrt{s_{NN}} = 2.76$ TeV, *Phys. Rev. Lett.* **117**, 182301 (2016).
- [20] H. Niemi, K. J. Eskola, and R. Paatelainen, Event-by-event fluctuations in a perturbative QCD + saturation + hydrodynamics model: Determining QCD matter shear viscosity in ultrarelativistic heavy-ion collisions, *Phys. Rev. C* **93**, 024907 (2016).
- [21] S. Gavin and M. Abdel-Aziz, Measuring Shear Viscosity Using Transverse Momentum Correlations in Relativistic Nuclear Collisions, *Phys. Rev. Lett.* **97**, 162302 (2006).
- [22] M. Sharma and C. A. Pruneau, Methods for the study of transverse momentum differential correlations, *Phys. Rev. C* **79**, 024905 (2009).
- [23] S. Gavin, G. Moschelli, and C. Zin, Rapidity correlation structure in nuclear collisions, *Phys. Rev. C* **94**, 024921 (2016).
- [24] S. Acharya *et al.* (ALICE Collaboration), Longitudinal and azimuthal evolution of two-particle transverse momentum correlations in Pb-Pb collisions at $\sqrt{s_{NN}} = 2.76$ TeV, *Phys. Lett. B* **804**, 135375 (2020).
- [25] V. Gonzalez, S. Basu, P. Ladron De Guevara, A. Marin, J. Pan, and C. A. Pruneau, Extraction of the specific shear viscosity of quark-gluon plasma from two-particle transverse momentum correlations, *Eur. Phys. J. C* **81**, 465 (2021).
- [26] B. B. Abelev *et al.* (ALICE Collaboration), Multiplicity dependence of the average transverse momentum in *pp*, *p*-Pb, and Pb-Pb collisions at the LHC, *Phys. Lett. B* **727**, 371 (2013).
- [27] B. B. Abelev *et al.* (ALICE Collaboration), Freeze-out radii extracted from three-pion cumulants in *pp*, *p*-Pb and Pb-Pb collisions at the LHC, *Phys. Lett. B* **739**, 139 (2014).
- [28] J. Adam *et al.* (ALICE Collaboration), Two-pion femtoscopy in *p*-Pb collisions at $\sqrt{s_{NN}} = 5.02$ TeV, *Phys. Rev. C* **91**, 034906 (2015).
- [29] A. M. Sirunyan *et al.* (CMS Collaboration), Bose-Einstein correlations in *pp*, *p*Pb, and PbPb collisions at $\sqrt{s_{NN}} = 0.9$ –7 TeV, *Phys. Rev. C* **97**, 064912 (2018).
- [30] U. W. Heinz and J. S. Moreland, Hydrodynamic flow in small systems or: “How the heck is it possible that a system emitting only a dozen particles can be described by fluid dynamics?”, *J. Phys.: Conf. Ser.* **1271**, 012018 (2019).
- [31] J. Adam *et al.* (ALICE Collaboration), Multiplicity and transverse momentum evolution of charge-dependent correlations in *pp*, *p*-Pb, and Pb-Pb collisions at the LHC, *Eur. Phys. J. C* **76**, 86 (2016).
- [32] S. Acharya *et al.* (ALICE Collaboration), Two-particle differential transverse momentum and number density correlations in *p*-Pb collisions at 5.02 TeV and Pb-Pb collisions at 2.76 TeV at the CERN Large Hadron Collider, *Phys. Rev. C* **100**, 044903 (2019).
- [33] V. Khachatryan *et al.* (CMS Collaboration), Observation of long-range near-side angular correlations in proton-proton collisions at the LHC, *J. High Energy Phys.* **09** (2010) 091.
- [34] V. Khachatryan *et al.* (CMS Collaboration), Measurement of Long-Range Near-Side Two-Particle Angular Correlations in *pp* Collisions at $\sqrt{s} = 13$ TeV, *Phys. Rev. Lett.* **116**, 172302 (2016).
- [35] G. Aad *et al.* (ATLAS Collaboration), Observation of Long-Range Elliptic Azimuthal Anisotropies in $\sqrt{s} = 13$ and 2.76 TeV *pp* Collisions with the ATLAS Detector, *Phys. Rev. Lett.* **116**, 172301 (2016).
- [36] K. Werner, B. Guiot, I. Karpenko, and T. Pierog, Analysing radial flow features in *p*-Pb and *p*-*p* collisions at several TeV by studying identified particle production in EPOS3, *Phys. Rev. C* **89**, 064903 (2014).
- [37] R. D. Weller and P. Romatschke, One fluid to rule them all: viscous hydrodynamic description of event-by-event central *p*+*p*, *p*+Pb and Pb+Pb collisions at $\sqrt{s} = 5.02$ TeV, *Phys. Lett. B* **774**, 351 (2017).
- [38] C. A. Pruneau, S. Gavin, and S. A. Voloshin, Transverse radial flow effects on two- and three-particle angular correlations, *Nucl. Phys. A* **802**, 107 (2008).
- [39] S. Gavin and G. Moschelli, Viscosity and the Soft Ridge at RHIC, *J. Phys. G: Nucl. Part. Phys.* **35**, 104084 (2008).
- [40] B. Abelev *et al.* (ALICE Collaboration), Long-range angular correlations on the near and away side in *p*-Pb collisions at $\sqrt{s_{NN}} = 5.02$ TeV, *Phys. Lett. B* **719**, 29 (2013).
- [41] K. Aamodt *et al.* (ALICE Collaboration), The ALICE experiment at the CERN LHC, *J. Instrum.* **3**, S08002 (2008).
- [42] B. Abelev *et al.* (ALICE Collaboration), Performance of the ALICE experiment at the CERN LHC, *Int. J. Mod. Phys. A* **29**, 1430044 (2014).
- [43] E. Abbas *et al.* (ALICE Collaboration), Performance of the ALICE VZERO system, *J. Instrum.* **8**, P10016 (2013).
- [44] S. Ravan, P. Pujahari, S. Prasad, and C. A. Pruneau, Correcting correlation function measurements, *Phys. Rev. C* **89**, 024906 (2014).
- [45] R. Brun, F. Bruyant, F. Carminati, S. Giani, M. Maire, A. McPherson, G. Patrick, and L. Urban, GEANT: Detector Description and Simulation Tool, Oct 1994, CERN Program Library, Report No. W5013 (unpublished), <http://cds.cern.ch/record/1082634>.
- [46] T. Sjöstrand, S. Mrenna, and P. Z. Skands, PYTHIA 6.4 physics and manual, *J. High Energy Phys.* **05** (2006) 026.
- [47] P. Z. Skands, Tuning Monte Carlo generators: The Perugia tunes, *Phys. Rev. D* **82**, 074018 (2010).
- [48] S. Roesler, R. Engel, and J. Ranft, The Monte Carlo event generator DPMJET-III, in *International Conference on Advanced Monte Carlo for Radiation Physics, Particle Transport Simulation and Applications (MC 2000)* (Springer, Berlin, 2001), pp. 1033–1038.
- [49] R. Barlow, Systematic errors: Facts and fictions, in *Proceedings of the Advanced Statistical Techniques in Particle Physics, Conference, Durham, UK, March 18–22, 2002* (University of Durham, Durham, UK, 2002), pp. 134–144.
- [50] S. Jeon and S. Pratt, Balance functions, correlations, charge fluctuations and interferometry, *Phys. Rev. C* **65**, 044902 (2002).
- [51] T. A. Trainor, Zero yield at minimum (ZYAM) method and v_2 : Underestimating jet yields from dihadron azimuth correlations, *Phys. Rev. C* **81**, 014905 (2010).
- [52] M. Mitrovski, T. Schuster, G. Graf, H. Petersen, and M. Bleicher, Charged-particle (pseudo-)rapidity distributions in $p + \bar{p}/p + p$ and Pb + Pb/Au + Au collisions from UrQMD calculations at energies available at the CERN Super Proton Synchrotron to the Large Hadron Collider, *Phys. Rev. C* **79**, 044901 (2009).
- [53] H. Petersen, Identified particle spectra and anisotropic flow in an event-by-event hybrid approach in Pb+Pb collisions at $\sqrt{s_{NN}} = 2.76$ TeV, *Phys. Rev. C* **84**, 034912 (2011).
- [54] S. Basu, T. K. Nayak, and K. Datta, Beam energy dependence of pseudorapidity distributions of charged particles produced

- in relativistic heavy-ion collisions, *Phys. Rev. C* **93**, 064902 (2016).
- [55] D. Solanki, P. Sorensen, S. Basu, R. Raniwala, and T. K. Nayak, Beam energy dependence of Elliptic and Triangular flow with the AMPT model, *Phys. Lett. B* **720**, 352 (2013).
- [56] K. Werner, Core-Corona Separation in Ultrarelativistic Heavy Ion Collisions, *Phys. Rev. Lett.* **98**, 152301 (2007).
- [57] S. Basu, S. Thakur, T. K. Nayak, and C. A. Pruneau, Multiplicity and pseudorapidity density distributions of charged particles produced in pp, pA and AA collisions at RHIC & LHC energies, *J. Phys. G: Nucl. Part. Phys.* **48**, 025103 (2021).
- [58] A. G. Knospe, C. Markert, K. Werner, J. Steinheimer, and M. Bleicher, Hadronic resonance production and interaction in partonic and hadronic matter in the EPOS3 model with and without the hadronic afterburner UrQMD, *Phys. Rev. C* **93**, 014911 (2016).
- [59] S. Basu, V. Gonzalez, J. Pan, A. Knospe, A. Marin, C. Markert, and C. Pruneau, Differential two-particle number and momentum correlations with the AMPT, UrQMD, and EPOS models in Pb-Pb collisions at $\sqrt{s_{NN}} = 2.76$ TeV, *Phys. Rev. C* **104**, 064902 (2021).
- [60] T. Sjöstrand, S. Mrenna, and P. Z. Skands, A Brief Introduction to PYTHIA 8.1, *Comput. Phys. Commun.* **178**, 852 (2008).
- [61] P. Skands, S. Carrazza, and J. Rojo, Tuning PYTHIA 8.1: the Monash 2013 Tune, *Eur. Phys. J. C* **74**, 3024 (2014).
- [62] X.-N. Wang and M. Gyulassy, HIJING: A Monte Carlo model for multiple jet production in pp, pA and AA collisions, *Phys. Rev. D* **44**, 3501 (1991).
- [63] B. Abelev *et al.* (ALICE Collaboration), Charge correlations using the balance function in Pb-Pb collisions at $\sqrt{s_{NN}} = 2.76$ TeV, *Phys. Lett. B* **723**, 267 (2013).
- [64] S. Acharya *et al.* (ALICE Collaboration), General balance functions of identified charged hadron pairs of (π , K, p) in Pb-Pb collisions at $\sqrt{s_{NN}} = 2.76$ TeV, *Phys. Lett. B* **833**, 137338 (2022).
- [65] J. Adams *et al.* (STAR Collaboration), Narrowing of the Balance Function with Centrality in Au+Au Collisions at $\sqrt{s_{NN}} = 130$ GeV, *Phys. Rev. Lett.* **90**, 172301 (2003).
- [66] M. M. Aggarwal *et al.* (STAR Collaboration), Balance Functions from Au+Au, d+Au, and p + p Collisions at $\sqrt{s_{NN}} = 200$ GeV, *Phys. Rev. C* **82**, 024905 (2010).
- [67] L. Adamczyk *et al.* (STAR Collaboration), Beam-energy dependence of charge balance functions from Au+Au collisions at energies available at the BNL Relativistic Heavy Ion Collider, *Phys. Rev. C* **94**, 024909 (2016).
- [68] F. Retiere and M. A. Lisa, Observable implications of geometrical and dynamical aspects of freeze-out in heavy ion collisions, *Phys. Rev. C* **70**, 044907 (2004).
- [69] B. Abelev *et al.* (ALICE Collaboration), Centrality dependence of π , K, and p production in Pb-Pb collisions at $\sqrt{s_{NN}} = 2.76$ TeV, *Phys. Rev. C* **88**, 044910 (2013).
- [70] S. Schlichting and S. Pratt, Charge conservation at energies available at the BNL Relativistic Heavy Ion Collider and contributions to local parity violation observables, *Phys. Rev. C* **83**, 014913 (2011).
- [71] S. Pratt and C. Plumberg, Charge balance functions for heavy-ion collisions at energies available at the CERN Large Hadron Collider, *Phys. Rev. C* **104**, 014906 (2021).
- [72] C. Loizides, J. Kamin, and D. d'Enterria, Improved Monte Carlo Glauber predictions at present and future nuclear colliders, *Phys. Rev. C* **97**, 054910 (2018); **99**, 019901(E) (2019)].
- [73] G. Agakishiev *et al.* (STAR Collaboration), Evolution of the differential transverse momentum correlation function with centrality in Au+Au collisions at $\sqrt{s_{NN}} = 200$ GeV, *Phys. Lett. B* **704**, 467 (2011).

S. Acharya¹²⁵, D. Adamová⁸⁶, A. Adler⁶⁹, G. Aglieri Rinella³², M. Agnello²⁹, N. Agrawal⁵⁰, Z. Ahammed¹³², S. Ahmad¹⁵, S. U. Ahn⁷⁰, I. Ahuja³⁷, A. Akindinov¹⁴⁰, M. Al-Turany⁹⁷, D. Aleksandrov¹⁴⁰, B. Alessandro⁵⁵, H. M. Alfanda⁶, R. Alfaro Molina⁶⁶, B. Ali¹⁵, A. Alici²⁵, N. Alizadehvandchali¹¹⁴, A. Alkin³², J. Alme²⁰, G. Alocco⁵¹, T. Alt⁶³, I. Altsybeev¹⁴⁰, M. N. Anaam⁶, C. Andrei⁴⁵, A. Andronic¹³⁵, V. Anguelov⁹⁴, F. Antinori⁵³, P. Antonioli⁵⁰, N. Apadula⁷⁴, L. Aphecetche¹⁰³, H. Appelshäuser⁶³, C. Arata⁷³, S. Arcelli²⁵, M. Aresti⁵¹, R. Arnaldi⁵⁵, I. C. Arsene¹⁹, M. Arslanok¹³⁷, A. Augustinus³², R. Averbeck⁹⁷, M. D. Azmi¹⁵, A. Badalà⁵², J. Bae¹⁰⁴, Y. W. Baek⁴⁰, X. Bai¹¹⁸, R. Bailhache⁶³, Y. Bailung⁴⁷, A. Balbino²⁹, A. Baldisseri¹²⁸, B. Balis², D. Banerjee⁴, Z. Banoo⁹¹, R. Barbera²⁶, F. Barile³¹, L. Barioglio⁹⁵, M. Barlou⁷⁸, G. G. Barnaföldi¹³⁶, L. S. Barnby⁸⁵, V. Barret¹²⁵, L. Barreto¹¹⁰, C. Bartels¹¹⁷, K. Barth³², E. Bartsch⁶³, N. Bastid¹²⁵, S. Basu⁷⁵, G. Batigne¹⁰³, D. Battistini⁹⁵, B. Batyunya¹⁴¹, D. Bauri⁴⁶, J. L. Bazo Alba¹⁰¹, I. G. Bearden⁸³, C. Beattie¹³⁷, P. Becht⁹⁷, D. Behera⁴⁷, I. Belikov¹²⁷, A. D. C. Bell Hechavarria¹³⁵, F. Bellini²⁵, R. Bellwied¹¹⁴, S. Belokurova¹⁴⁰, V. Belyaev¹⁴⁰, G. Bencedi¹³⁶, S. Beole²⁴, A. Bercuci⁴⁵, Y. Berdnikov¹⁴⁰, A. Berdnikova⁹⁴, L. Bergmann⁹⁴, M. G. Besoiu⁶², L. Betev³², P. P. Bhaduri¹³², A. Bhasin⁹¹, M. A. Bhat⁴, B. Bhattacharjee⁴¹, L. Bianchi²⁴, N. Bianchi⁴⁸, J. Bielčik³⁵, J. Bielčiková⁸⁶, J. Biernat¹⁰⁷, A. P. Bigot¹²⁷, A. Bilandzic⁹⁵, G. Biro¹³⁶, S. Biswas⁴, N. Bize¹⁰³, J. T. Blair¹⁰⁸, D. Blau¹⁴⁰, M. B. Blidaru⁹⁷, N. Bluhme³⁸, C. Blume⁶³, G. Boca^{21,54}, F. Bock⁸⁷, T. Bodova²⁰, A. Bogdanov¹⁴⁰, S. Boi²², J. Bok⁵⁷, L. Boldizsár¹³⁶, A. Bolozdynya¹⁴⁰, M. Bombara³⁷, P. M. Bond³², G. Bonomi^{131,54}, H. Borel¹²⁸, A. Borissov¹⁴⁰, A. G. Borquez Carcamo⁹⁴, H. Bossi¹³⁷, E. Botta²⁴, Y. E. M. Bouziani⁶³, L. Bratrud⁶³, P. Braun-Munzinger⁹⁷, M. Bregant¹¹⁰, M. Broz³⁵, G. E. Bruno^{96,31}, M. D. Buckland²³, D. Budnikov¹⁴⁰, H. Buesching⁶³, S. Bufalino²⁹, O. Bugnon¹⁰³, P. Buhler¹⁰², Z. Buthelezi^{67,121}, S. A. Bysiak¹⁰⁷, M. Cai⁶, H. Caines¹³⁷, A. Caliva⁹⁷, E. Calvo Villar¹⁰¹, J. M. M. Camacho¹⁰⁹, P. Camerini²³, F. D. M. Canedo¹¹⁰, M. Carabas¹²⁴, A. A. Carballo³², F. Carnesecchi³², R. Caron¹²⁶, L. A. D. Carvalho¹¹⁰, J. Castillo Castellanos¹²⁸, F. Catalano^{24,29}, C. Ceballos Sanchez¹⁴¹, I. Chakaberia⁷⁴, P. Chakraborty⁴⁶, S. Chandra¹³², S. Chapeland³², M. Chartier¹¹⁷, S. Chattopadhyay¹³², S. Chattopadhyay⁹⁹, T. G. Chavez⁴⁴

- T. Cheng ^{97,6} C. Cheshkov ¹²⁶ B. Cheynis ¹²⁶ V. Chibante Barroso ³² D. D. Chinellato ¹¹¹ E. S. Chizzali ^{95,a}
 J. Cho ⁵⁷ S. Cho ⁵⁷ P. Chochula ³² P. Christakoglou ⁸⁴ C. H. Christensen ⁸³ P. Christiansen ⁷⁵ T. Chujo ¹²³
 M. Ciacco ²⁹ C. Cicalo ⁵¹ F. Cindolo ⁵⁰ M. R. Ciupek ⁹⁷ G. Clai ^{50,b} F. Colamaria ⁴⁹ J. S. Colburn ¹⁰⁰ D. Colella ^{96,31}
 M. Colocci ³² M. Concas ^{55,c} G. Conesa Balbastre ⁷³ Z. Conesa del Valle ⁷² G. Contin ²³ J. G. Contreras ³⁵
 M. L. Coquet ¹²⁸ T. M. Cormier ^{87,d} P. Cortese ^{130,55} M. R. Cosentino ¹¹² F. Costa ³² S. Costanza ^{21,54} C. Cot ⁷²
 J. Crkovská ⁹⁴ P. Crochet ¹²⁵ R. Cruz-Torres ⁷⁴ E. Cuautle ⁶⁴ P. Cui ⁶ A. Dainese ⁵³ M. C. Danisch ⁹⁴ A. Danu ⁶²
 P. Das ⁸⁰ P. Das ⁴ S. Das ⁴ A. R. Dash ¹³⁵ S. Dash ⁴⁶ A. De Caro ²⁸ G. de Cataldo ⁴⁹ J. de Cuveland ³⁸
 A. De Falco ²² D. De Gruttola ²⁸ N. De Marco ⁵⁵ C. De Martin ²³ S. De Pasquale ²⁸ S. Deb ⁴⁷ R. J. Debski ²
 K. R. Deja ¹³³ R. Del Grande ⁹⁵ L. Dello Stritto ²⁸ W. Deng ⁶ P. Dhankher ¹⁸ D. Di Bari ³¹ A. Di Mauro ³²
 R. A. Diaz ^{141,7} T. Dietel ¹¹³ Y. Ding ^{126,6} R. Divià ³² D. U. Dixit ¹⁸ Ø. Djuvsland ²⁰ U. Dmitrieva ¹⁴⁰
 A. Dobrin ⁶² B. Dönigus ⁶³ J. M. Dubinski ¹³³ A. Dubla ⁹⁷ S. Dudi ⁹⁰ P. Dupieux ¹²⁵ M. Durkac ¹⁰⁶ N. Dzalaiova ¹²
 T. M. Eder ¹³⁵ R. J. Ehlers ⁸⁷ V. N. Eikeland ²⁰ F. Eisenhut ⁶³ D. Elia ⁴⁹ B. Erasmus ¹⁰³ F. Ercolessi ²⁵
 F. Erhardt ⁸⁹ M. R. Ersdal ²⁰ B. Espagnon ⁷² G. Eulisse ³² D. Evans ¹⁰⁰ S. Evdokimov ¹⁴⁰ L. Fabbietti ⁹⁵
 M. Faggin ²⁷ J. Faivre ⁷³ F. Fan ⁶ W. Fan ⁷⁴ A. Fantoni ⁴⁸ M. Fasel ⁸⁷ P. Fedchio ²⁹ A. Feliciello ⁵⁵
 G. Feofilov ¹⁴⁰ A. Fernández Téllez ⁴⁴ L. Ferrandi ¹¹⁰ M. B. Ferrer ³² A. Ferrero ¹²⁸ C. Ferrero ⁵⁵ A. Ferretti ²⁴
 V. J. G. Feuillard ⁹⁴ V. Filova ³⁵ D. Finogeev ¹⁴⁰ F. M. Fionda ⁵¹ F. Flor ¹¹⁴ A. N. Flores ¹⁰⁸ S. Foertsch ⁶⁷
 I. Fokin ⁹⁴ S. Fokin ¹⁴⁰ E. Fragiaco ⁵⁶ E. Frajna ¹³⁶ U. Fuchs ³² N. Funicello ²⁸ C. Furget ⁷³ A. Furs ¹⁴⁰
 T. Fusayasu ⁹⁸ J. J. Gaardhøje ⁸³ M. Gagliardi ²⁴ A. M. Gago ¹⁰¹ C. D. Galvan ¹⁰⁹ D. R. Gangadharan ¹¹⁴
 P. Ganoti ⁷⁸ C. Garabatos ⁹⁷ J. R. A. Garcia ⁴⁴ E. Garcia-Solis ⁹ K. Garg ¹⁰³ C. Gargiulo ³² K. Garner ¹³⁵
 P. Gasik ⁹⁷ A. Gautam ¹¹⁶ M. B. Gay Ducati ⁶⁵ M. Germain ¹⁰³ C. Ghosh ¹³² M. Giacalone ²⁵ P. Giubellino ^{97,55}
 P. Giubilato ²⁷ A. M. C. Glaenger ¹²⁸ P. Gläsel ⁹⁴ E. Glimos ¹²⁰ D. J. Q. Goh ⁷⁶ V. Gonzalez ¹³⁴
 L. H. González-Trueba ⁶⁶ M. Gorgon ² S. Gotovac ³³ V. Grabski ⁶⁶ L. K. Graczykowski ¹³³ E. Grecka ⁸⁶
 A. Grelli ⁵⁸ C. Grigoras ³² V. Grigoriev ¹⁴⁰ S. Grigoryan ^{141,1} F. Grosa ³² J. F. Grosse-Oetringhaus ³² R. Grosso ⁹⁷
 D. Grund ³⁵ G. G. Guardiano ¹¹¹ R. Guernane ⁷³ M. Guilbaud ¹⁰³ K. Gulbrandsen ⁸³ T. Gundem ⁶³ T. Gunji ¹²²
 W. Guo ⁶ A. Gupta ⁹¹ R. Gupta ⁹¹ S. P. Guzman ⁴⁴ L. Gyulai ¹³⁶ M. K. Habib ⁹⁷ C. Hadjidakis ⁷² F. U. Haider ⁹¹
 H. Hamagaki ⁷⁶ A. Hamdi ⁷⁴ M. Hamid ⁶ Y. Han ¹³⁸ R. Hannigan ¹⁰⁸ M. R. Haque ¹³³ J. W. Harris ¹³⁷
 A. Harton ⁹ H. Hassan ⁸⁷ D. Hatzifotiadou ⁵⁰ P. Hauer ⁴² L. B. Havener ¹³⁷ S. T. Heckel ⁹⁵ E. Hellbär ⁹⁷
 H. Helstrup ³⁴ M. Hemmer ⁶³ T. Herman ³⁵ G. Herrera Corral ⁸ F. Herrmann ¹³⁵ S. Herrmann ¹²⁶ K. F. Hetland ³⁴
 B. Heybeck ⁶³ H. Hillemanns ³² C. Hills ¹¹⁷ B. Hippolyte ¹²⁷ B. Hofman ⁵⁸ B. Hohlweger ⁸⁴ G. H. Hong ¹³⁸
 M. Horst ⁹⁵ A. Horzyk ² R. Hosokawa ¹⁴ Y. Hou ⁶ P. Hristov ³² C. Hughes ¹²⁰ P. Huhn ⁶³ L. M. Huhta ¹¹⁵
 C. V. Hulse ⁷² T. J. Humanic ⁸⁸ A. Hutson ¹¹⁴ D. Hutter ³⁸ J. P. Iddon ¹¹⁷ R. Ilkaev ¹⁴⁰ H. Ilyas ¹³ M. Inaba ¹²³
 G. M. Innocenti ³² M. Ippolitov ¹⁴⁰ A. Isakov ⁸⁶ T. Isidori ¹¹⁶ M. S. Islam ⁹⁹ M. Ivanov ¹² M. Ivanov ⁹⁷
 V. Ivanov ¹⁴⁰ M. Jablonski ² B. Jacak ⁷⁴ N. Jacazio ³² P. M. Jacobs ⁷⁴ S. Jadlovská ¹⁰⁶ J. Jadlovsky ¹⁰⁶ S. Jaelani ⁸²
 L. Jaffe ³⁸ C. Jahnke ¹¹¹ M. J. Jakubowska ¹³³ M. A. Janik ¹³³ T. Janson ⁶⁹ M. Jercic ⁸⁹ S. Jia ¹⁰ A. A. P. Jimenez ⁶⁴
 F. Jonas ⁸⁷ J. M. Jowett ^{32,97} J. Jung ⁶³ M. Jung ⁶³ A. Junique ³² A. Jusko ¹⁰⁰ M. J. Kabus ^{32,133} J. Kaewjai ¹⁰⁵
 P. Kalinak ⁵⁹ A. S. Kalteyer ⁹⁷ A. Kalweit ³² V. Kaplin ¹⁴⁰ A. Karasu Uysal ⁷¹ D. Karatovic ⁸⁹ O. Karavichev ¹⁴⁰
 T. Karavicheva ¹⁴⁰ P. Karczmarczyk ¹³³ E. Karpechev ¹⁴⁰ U. Keschull ⁶⁹ R. Keidel ¹³⁹ D. L. D. Keijdener ⁵⁸
 M. Keil ³² B. Ketzer ⁴² A. M. Khan ⁶ S. Khan ¹⁵ A. Khanzadeev ¹⁴⁰ Y. Kharlov ¹⁴⁰ A. Khatun ^{116,15}
 A. Khuntia ¹⁰⁷ M. B. Kidson ¹¹³ B. Kileng ³⁴ B. Kim ¹⁶ C. Kim ¹⁶ D. J. Kim ¹¹⁵ E. J. Kim ⁶⁸ J. Kim ¹³⁸
 J. S. Kim ⁴⁰ J. Kim ⁹⁴ J. Kim ⁶⁸ M. Kim ^{18,94} S. Kim ¹⁷ T. Kim ¹³⁸ K. Kimura ⁹² S. Kirsch ⁶³ I. Kisel ³⁸
 S. Kiselev ¹⁴⁰ A. Kisiel ¹³³ J. P. Kitowski ² J. L. Klay ⁵ J. Klein ³² S. Klein ⁷⁴ C. Klein-Bösing ¹³⁵ M. Kleiner ⁶³
 T. Klemenz ⁹⁵ A. Kluge ³² A. G. Knospe ¹¹⁴ C. Kobdaj ¹⁰⁵ T. Kollegger ⁹⁷ A. Kondratyev ¹⁴¹ N. Kondratyeva ¹⁴⁰
 E. Kondratyuk ¹⁴⁰ J. König ⁶³ S. A. Konigstorfer ⁹⁵ P. J. Konopka ³² G. Kornakov ¹³³ S. D. Koryciak ²
 A. Kotliarov ⁸⁶ V. Kovalenko ¹⁴⁰ M. Kowalski ¹⁰⁷ V. Kozhuharov ³⁶ I. Králik ⁵⁹ A. Kravčáková ³⁷ L. Kreis ⁹⁷
 M. Krivda ^{100,59} F. Krizek ⁸⁶ K. Krizkova Gajdosova ³⁵ M. Kroesen ⁹⁴ M. Krüger ⁶³ D. M. Krupova ³⁵
 E. Kryshen ¹⁴⁰ V. Kučera ³² C. Kuhn ¹²⁷ P. G. Kuijer ⁸⁴ T. Kumaoka ¹²³ D. Kumar ¹³² L. Kumar ⁹⁰ N. Kumar ⁹⁰
 S. Kumar ³¹ S. Kundu ³² P. Kurashvili ⁷⁹ A. Kurepin ¹⁴⁰ A. B. Kurepin ¹⁴⁰ A. Kuryakin ¹⁴⁰ S. Kushpil ⁸⁶
 J. Kvapil ¹⁰⁰ M. J. Kweon ⁵⁷ J. Y. Kwon ⁵⁷ Y. Kwon ¹³⁸ S. L. La Pointe ³⁸ P. La Rocca ²⁶ P. Ladron de Guevara ⁶⁶
 Y. S. Lai ⁷⁴ A. Lakrathok ¹⁰⁵ M. Lamanna ³² R. Langoy ¹¹⁹ P. Larionov ³² E. Laudi ³² L. Lautner ^{32,95}
 R. Lavicka ¹⁰² T. Lazareva ¹⁴⁰ R. Lea ^{131,54} H. Lee ¹⁰⁴ G. Legras ¹³⁵ J. Lehrbach ³⁸ R. C. Lemmon ⁸⁵
 I. León Monzón ¹⁰⁹ M. M. Lesch ⁹⁵ E. D. Lesser ¹⁸ M. Lettrich ⁹⁵ P. Lévai ¹³⁶ X. Li ¹⁰ X. L. Li ⁶ J. Lien ¹¹⁹
 R. Lietava ¹⁰⁰ B. Lim ^{24,16} S. H. Lim ¹⁶ V. Lindenstruth ³⁸ A. Lindner ⁴⁵ C. Lippmann ⁹⁷ A. Liu ¹⁸ D. H. Liu ⁶
 J. Liu ¹¹⁷ I. M. Lofnes ²⁰ C. Loizides ⁸⁷ S. Lokos ¹⁰⁷ J. Lomker ⁵⁸ P. Loncar ³³ J. A. Lopez ⁹⁴ X. Lopez ¹²⁵
 E. López Torres ⁷ P. Lu ^{97,118} J. R. Luhder ¹³⁵ M. Lunardon ²⁷ G. Luparello ⁵⁶ Y. G. Ma ³⁹ A. Maevskaya ¹⁴⁰
 M. Mager ³² T. Mahmoud ⁴² A. Maire ¹²⁷ M. V. Makariev ³⁶ M. Malaev ¹⁴⁰ G. Malfattore ²⁵ N. M. Malik ⁹¹
 Q. W. Malik ¹⁹ S. K. Malik ⁹¹ L. Malinina ^{141,e} D. Mal'Kevich ¹⁴⁰ D. Mallick ⁸⁰ N. Mallick ⁴⁷ G. Mandaglio ^{30,52}
 V. Manko ¹⁴⁰ F. Manso ¹²⁵ V. Manzari ⁴⁹ Y. Mao ⁶ G. V. Margagliotti ²³ A. Margotti ⁵⁰ A. Marín ⁹⁷
 C. Markert ¹⁰⁸ P. Martinengo ³² J. L. Martinez ¹¹⁴ M. I. Martínez ⁴⁴ G. Martínez García ¹⁰³ S. Masciocchi ⁹⁷

- M. Maserà²⁴ A. Masoni⁵¹ L. Massacrier⁷² A. Mastroserio^{129,49} O. Matonoha⁷⁵ P. F. T. Matuoka¹¹⁰
A. Matyja¹⁰⁷ C. Mayer¹⁰⁷ A. L. Mazuecos³² F. Mazzaschi²⁴ M. Mazzilli³² J. E. Mdhuli¹²¹ A. F. Mechler⁶³
Y. Melikyan^{43,140} A. Menchaca-Rocha⁶⁶ E. Meninno^{102,28} A. S. Menon¹¹⁴ M. Meres¹² S. Mhlanga^{113,67}
Y. Miake¹²³ L. Micheletti⁵⁵ L. C. Migliorin¹²⁶ D. L. Mihaylov⁹⁵ K. Mikhaylov^{141,140} A. N. Mishra¹³⁶
D. Miśkowiec⁹⁷ A. Modak⁴ A. P. Mohanty⁵⁸ B. Mohanty⁸⁰ M. Mohisin Khan^{15,f} M. A. Molander⁴³
Z. Moravcova⁸³ C. Mordasini⁹⁵ D. A. Moreira De Godoy¹³⁵ I. Morozov¹⁴⁰ A. Morsch³² T. Mrnjavac³²
V. Muccifora⁴⁸ S. Muhuri¹³² J. D. Mulligan⁷⁴ A. Mulliri²² M. G. Munhoz¹¹⁰ R. H. Munzer⁶³ H. Murakami¹²²
S. Murray¹¹³ L. Musa³² J. Musinsky⁵⁹ J. W. Myrcha¹³³ B. Naik¹²¹ A. I. Nambrath¹⁸ B. K. Nandi⁴⁶
R. Nania⁵⁰ E. Nappi⁴⁹ A. F. Nassirpour⁷⁵ A. Nath⁹⁴ C. Nattrass¹²⁰ M. N. Naydenov³⁶ A. Neagu¹⁹ A. Negru¹²⁴
L. Nellen⁶⁴ S. V. Nesbo³⁴ G. Neskovic³⁸ D. Nesterov¹⁴⁰ B. S. Nielsen⁸³ E. G. Nielsen⁸³ S. Nikolaev¹⁴⁰
S. Nikulin¹⁴⁰ V. Nikulin¹⁴⁰ F. Noferini⁵⁰ S. Noh¹¹ P. Nomokonov¹⁴¹ J. Norman¹¹⁷ N. Novitzky¹²³
P. Nowakowski¹³³ A. Nyanin¹⁴⁰ J. Nystrand²⁰ M. Ogino⁷⁶ A. Ohlson⁷⁵ V. A. Okorokov¹⁴⁰ J. Oleniacz¹³³
A. C. Oliveira Da Silva¹²⁰ M. H. Oliver¹³⁷ A. Onnerstad¹¹⁵ C. Oppedisano⁵⁵ A. Ortiz Velasquez⁶⁴
J. Otwinowski¹⁰⁷ M. Oya⁹² K. Oyama⁷⁶ Y. Pachmayer⁹⁴ S. Padhan⁴⁶ D. Pagano^{131,54} G. Paic⁶⁴
A. Palasciano⁴⁹ S. Panebianco¹²⁸ H. Park¹²³ H. Park¹⁰⁴ J. Park⁵⁷ J. E. Parkkila³² R. N. Patra⁹¹ B. Paul²²
H. Pei⁶ T. Peitzmann⁵⁸ X. Peng⁶ M. Pennisi²⁴ L. G. Pereira⁶⁵ D. Peresunko¹⁴⁰ G. M. Perez⁷ S. Perrin¹²⁸
Y. Pestov¹⁴⁰ V. Petráček³⁵ V. Petrov¹⁴⁰ M. Petrovici⁴⁵ R. P. Pezzi^{103,65} S. Piano⁵⁶ M. Pikna¹² P. Pillot¹⁰³
O. Pinazza^{50,32} L. Pinsky¹¹⁴ C. Pinto⁹⁵ S. Pisano⁴⁸ M. Płoskoń⁷⁴ M. Planinic⁸⁹ F. Pliquett⁶³ M. G. Poghosyan⁸⁷
B. Polichtchouk¹⁴⁰ S. Politano²⁹ N. Poljak⁸⁹ A. Pop⁴⁵ S. Porteboeuf-Houssais¹²⁵ V. Pozdniakov¹⁴¹
K. K. Pradhan⁴⁷ S. K. Prasad⁴ S. Prasad⁴⁷ R. Preghenella⁵⁰ F. Prino⁵⁵ C. A. Pruneau¹³⁴ I. Pshenichnov¹⁴⁰
M. Puccio³² S. Pucillo²⁴ Z. Pugalova¹⁰⁶ S. Qiu⁸⁴ L. Quaglia²⁴ R. E. Quishpe¹¹⁴ S. Ragoni^{14,100}
A. Rakotozafindrabe¹²⁸ L. Ramello^{130,55} F. Rami¹²⁷ S. A. R. Ramirez⁴⁴ T. A. Rancien⁷³ M. Rasa²⁶
S. S. Räsänen⁴³ R. Rath⁵⁰ M. P. Rauch²⁰ I. Ravasenga⁸⁴ K. F. Read^{87,120} C. Reckziegel¹¹² A. R. Redelbach³⁸
K. Redlich^{79,g} C. A. Reetz⁹⁷ A. Rehman²⁰ F. Reidt³² H. A. Reme-Ness³⁴ Z. Rescakova³⁷ K. Reygers⁹⁴
A. Riabov¹⁴⁰ V. Riabov¹⁴⁰ R. Ricci²⁸ M. Richter¹⁹ A. A. Riedel⁹⁵ W. Riegler³² C. Ristea⁶²
M. Rodríguez Cahuantzi⁴⁴ K. Røed¹⁹ R. Rogalev¹⁴⁰ E. Rogochaya¹⁴¹ T. S. Rogoschinski⁶³ D. Rohr³²
D. Röhrich²⁰ P. F. Rojas⁴⁴ S. Rojas Torres³⁵ P. S. Rokita¹³³ G. Romanenko¹⁴¹ F. Ronchetti⁴⁸ A. Rosano^{30,52}
E. D. Rosas⁶⁴ K. Roslon¹³³ A. Rossi⁵³ A. Roy⁴⁷ S. Roy⁴⁶ N. Rubini²⁵ O. V. Rueda^{114,75} D. Ruggiano¹³³
R. Rui²³ B. Rumyantsev¹⁴¹ P. G. Russek² R. Russo⁸⁴ A. Rustamov⁸¹ E. Ryabinkin¹⁴⁰ Y. Ryabov¹⁴⁰
A. Rybicki¹⁰⁷ H. Rytönen¹¹⁵ W. Rzeska¹³³ O. A. M. Saarimäki⁴³ R. Sadek¹⁰³ S. Sadhu³¹ S. Sadovsky¹⁴⁰
J. Saetre²⁰ K. Šafařík³⁵ S. K. Saha⁴ S. Saha⁸⁰ B. Sahoo⁴⁶ R. Sahoo⁴⁷ S. Sahoo⁶⁰ D. Sahu⁴⁷ P. K. Sahu⁶⁰
J. Saini¹³² K. Sajdakova³⁷ S. Sakai¹²³ M. P. Salvan⁹⁷ S. Sambyal⁹¹ I. Sanna^{32,95} T. B. Saramela¹¹⁰
D. Sarkar¹³⁴ N. Sarkar¹³² P. Sarma⁴¹ V. Sarritzu²² V. M. Sarti⁹⁵ M. H. P. Sas¹³⁷ J. Schambach⁸⁷ H. S. Scheid⁶³
C. Schiaua⁴⁵ R. Schicker⁹⁴ A. Schmah⁹⁴ C. Schmidt⁹⁷ H. R. Schmidt⁹³ M. O. Schmidt³² M. Schmidt⁹³
N. V. Schmidt⁸⁷ A. R. Schmier¹²⁰ R. Schotter¹²⁷ A. Schröter³⁸ J. Schukraft³² K. Schwarz⁹⁷ K. Schweda⁹⁷
G. Scioli²⁵ E. Scomparin⁵⁵ J. E. Seger¹⁴ Y. Sekiguchi¹²² D. Sekihata¹²² I. Selyuzhenkov^{97,140} S. Senyukov¹²⁷
J. J. Seo⁵⁷ D. Serebryakov¹⁴⁰ L. Šerkšnytė⁹⁵ A. Sevcenco⁶² T. J. Shaba⁶⁷ A. Shabetai¹⁰³ R. Shahoyan³²
A. Shangaraev¹⁴⁰ A. Sharma⁹⁰ B. Sharma⁹¹ D. Sharma⁴⁶ H. Sharma¹⁰⁷ M. Sharma⁹¹ S. Sharma⁷⁶
S. Sharma⁹¹ U. Sharma⁹¹ A. Shatat⁷² O. Sheibani¹¹⁴ K. Shigaki⁹² M. Shimomura⁷⁷ J. Shin¹¹ S. Shirinkin¹⁴⁰
Q. Shou³⁹ Y. Sibiriak¹⁴⁰ S. Siddhanta⁵¹ T. Siemiarczuk⁷⁹ T. F. Silva¹¹⁰ D. Silvermyr⁷⁵
T. Simantathammakul¹⁰⁵ R. Simeonov³⁶ B. Singh⁹¹ B. Singh⁹⁵ R. Singh⁸⁰ R. Singh⁹¹ R. Singh⁴⁷ S. Singh¹⁵
V. K. Singh¹³² V. Singhal¹³² T. Sinha⁹⁹ B. Sitar¹² M. Sitta^{130,55} T. B. Skaali¹⁹ G. Skorodumovs⁹⁴
M. Słupecki⁴³ N. Smirnov¹³⁷ R. J. M. Snellings⁵⁸ E. H. Solheim¹⁹ J. Song¹¹⁴ A. Songmoonak¹⁰⁵ F. Soramel²⁷
R. Spijkers⁸⁴ I. Sputowska¹⁰⁷ J. Staa⁷⁵ J. Stachel⁹⁴ I. Stan⁶² P. J. Steffanic¹²⁰ S. F. Stiefelmaier⁹⁴
D. Stocco¹⁰³ I. Storehaug¹⁹ P. Stratmann¹³⁵ S. Strazzi²⁵ C. P. Stylianidis⁸⁴ A. A. P. Suaide¹¹⁰ C. Suire⁷²
M. Sukhanov¹⁴⁰ M. Suljic³² R. Sultanov¹⁴⁰ V. Sumberia⁹¹ S. Sumowidagdo⁸² S. Swain⁶⁰ I. Szarka¹²
S. F. Taghavi⁹⁵ G. Taillepied⁹⁷ J. Takahashi¹¹¹ G. J. Tambave²⁰ S. Tang^{125,6} Z. Tang¹¹⁸ J. D. Tapia Takaki¹¹⁶
N. Tapus¹²⁴ L. A. Tarasovicova¹³⁵ M. G. Tarzila⁴⁵ G. F. Tassielli³¹ A. Tauro³² G. Tejada Muñoz⁴⁴ A. Telesca³²
L. Terlizzi²⁴ C. Terrevoli¹¹⁴ G. Tersimonov³ S. Thakur⁴ D. Thomas¹⁰⁸ A. Tikhonov¹⁴⁰ A. R. Timmins¹¹⁴
M. Tkacik¹⁰⁶ T. Tkacik¹⁰⁶ A. Toia⁶³ R. Tokumoto⁹² N. Topilskaya¹⁴⁰ M. Toppi⁴⁸ F. Torales-Acosta¹⁸ T. Tork⁷²
A. G. Torres Ramos³¹ A. Trifiró^{30,52} A. S. Triolo^{30,52} S. Tripathy⁵⁰ T. Tripathy⁴⁶ S. Trogolo³² V. Trubnikov³
W. H. Trzaska¹¹⁵ T. P. Trzcinski¹³³ A. Tumkin¹⁴⁰ R. Turrisi⁵³ T. S. Tveter¹⁹ K. Ullaland²⁰ B. Ulukutlu⁹⁵
A. Uras¹²⁶ M. Urioni^{54,131} G. L. Usai²² M. Vala³⁷ N. Valle²¹ L. V. R. van Doremalen⁵⁸ M. van Leeuwen⁸⁴
C. A. van Veen⁹⁴ R. J. G. van Weelden⁸⁴ P. Vande Vyvre³² D. Varga¹³⁶ Z. Varga¹³⁶ M. Vasileiou⁷⁸
A. Vasiliev¹⁴⁰ O. Vázquez Doce⁴⁸ V. Vechernin¹⁴⁰ E. Vercellin²⁴ S. Vergara Limón⁴⁴ L. Vermunt⁹⁷
R. Vértési¹³⁶ M. Verweij⁵⁸ L. Vickovic³³ Z. Vilakazi¹²¹ O. Villalobos Baillie¹⁰⁰ G. Vino⁴⁹ A. Vinogradov¹⁴⁰
T. Virgili²⁸ V. Vislavicius⁸³ A. Vodopyanov¹⁴¹ B. Volkel³² M. A. Völkl⁹⁴ K. Voloshin¹⁴⁰ S. A. Voloshin¹³⁴
G. Volpe³¹ B. von Haller³² I. Vorobyev⁹⁵ N. Vozniuk¹⁴⁰ J. Vrláková³⁷ C. Wang³⁹ D. Wang³⁹ Y. Wang³⁹

A. Wegrzynek³², F. T. Weiglhofer³⁸, S. C. Wenzel³², J. P. Wessels¹³⁵, S. L. Weyhmiller¹³⁷, J. Wiechula⁶³, J. Wikne¹⁹, G. Wilk⁷⁹, J. Wilkinson⁹⁷, G. A. Willems¹³⁵, B. Windelband⁹⁴, M. Winn¹²⁸, J. R. Wright¹⁰⁸, W. Wu³⁹, Y. Wu¹¹⁸, R. Xu⁶, A. Yadav⁴², A. K. Yadav¹³², S. Yalcin⁷¹, Y. Yamaguchi⁹², S. Yang²⁰, S. Yano⁹², Z. Yin⁶, I.-K. Yoo¹⁶, J. H. Yoon⁵⁷, S. Yuan²⁰, A. Yuncu⁹⁴, V. Zaccolo²³, C. Zampolli³², F. Zanone⁹⁴, N. Zardoshti^{32,100}, A. Zarochentsev¹⁴⁰, P. Závada⁶¹, N. Zaviyalov¹⁴⁰, M. Zhalov¹⁴⁰, B. Zhang⁶, L. Zhang³⁹, S. Zhang³⁹, X. Zhang⁶, Y. Zhang¹¹⁸, Z. Zhang⁶, M. Zhao¹⁰, V. Zherebchevskii¹⁴⁰, Y. Zhi¹⁰, D. Zhou⁶, Y. Zhou⁸³, J. Zhu^{97,6}, Y. Zhu⁶, S. C. Zugeravel⁵⁵ and N. Zurlo^{131,54}

(ALICE Collaboration)

- ¹A. I. Alikhanyan National Science Laboratory (Yerevan Physics Institute) Foundation, Yerevan, Armenia
²AGH University of Science and Technology, Cracow, Poland
³Bogolyubov Institute for Theoretical Physics, National Academy of Sciences of Ukraine, Kiev, Ukraine
⁴Department of Physics and Centre for Astroparticle Physics and Space Science (CAPSS), Bose Institute, Kolkata, India
⁵California Polytechnic State University, San Luis Obispo, California, USA
⁶Central China Normal University, Wuhan, China
⁷Centro de Aplicaciones Tecnológicas y Desarrollo Nuclear (CEADEN), Havana, Cuba
⁸Centro de Investigación y de Estudios Avanzados (CINVESTAV), Mexico City and Mérida, Mexico
⁹Chicago State University, Chicago, Illinois, USA
¹⁰China Institute of Atomic Energy, Beijing, China
¹¹Chungbuk National University, Cheongju, Republic of Korea
¹²Faculty of Mathematics, Physics and Informatics, Comenius University Bratislava, Bratislava, Slovak Republic
¹³COMSATS University Islamabad, Islamabad, Pakistan
¹⁴Creighton University, Omaha, Nebraska, USA
¹⁵Department of Physics, Aligarh Muslim University, Aligarh, India
¹⁶Department of Physics, Pusan National University, Pusan, Republic of Korea
¹⁷Department of Physics, Sejong University, Seoul, Republic of Korea
¹⁸Department of Physics, University of California, Berkeley, California, USA
¹⁹Department of Physics, University of Oslo, Oslo, Norway
²⁰Department of Physics and Technology, University of Bergen, Bergen, Norway
²¹Dipartimento di Fisica, Università di Pavia, Pavia, Italy
²²Dipartimento di Fisica dell'Università and Sezione INFN, Cagliari, Italy
²³Dipartimento di Fisica dell'Università and Sezione INFN, Trieste, Italy
²⁴Dipartimento di Fisica dell'Università and Sezione INFN, Turin, Italy
²⁵Dipartimento di Fisica e Astronomia dell'Università and Sezione INFN, Bologna, Italy
²⁶Dipartimento di Fisica e Astronomia dell'Università and Sezione INFN, Catania, Italy
²⁷Dipartimento di Fisica e Astronomia dell'Università and Sezione INFN, Padova, Italy
²⁸Dipartimento di Fisica 'E. R. Caianiello' dell'Università and Gruppo Collegato INFN, Salerno, Italy
²⁹Dipartimento DISAT del Politecnico and Sezione INFN, Turin, Italy
³⁰Dipartimento di Scienze MIFT, Università di Messina, Messina, Italy
³¹Dipartimento Interateneo di Fisica 'M. Merlin' and Sezione INFN, Bari, Italy
³²European Organization for Nuclear Research (CERN), Geneva, Switzerland
³³Faculty of Electrical Engineering, Mechanical Engineering and Naval Architecture, University of Split, Split, Croatia
³⁴Faculty of Engineering and Science, Western Norway University of Applied Sciences, Bergen, Norway
³⁵Faculty of Nuclear Sciences and Physical Engineering, Czech Technical University in Prague, Prague, Czech Republic
³⁶Faculty of Physics, Sofia University, Sofia, Bulgaria
³⁷Faculty of Science, P. J. Šafárik University, Košice, Slovak Republic
³⁸Frankfurt Institute for Advanced Studies, Johann Wolfgang Goethe-Universität Frankfurt, Frankfurt, Germany
³⁹Fudan University, Shanghai, China
⁴⁰Gangneung-Wonju National University, Gangneung, Republic of Korea
⁴¹Department of Physics, Gauhati University, Guwahati, India
⁴²Helmholtz-Institut für Strahlen- und Kernphysik, Rheinische Friedrich-Wilhelms-Universität Bonn, Bonn, Germany
⁴³Helsinki Institute of Physics (HIP), Helsinki, Finland
⁴⁴High Energy Physics Group, Universidad Autónoma de Puebla, Puebla, Mexico
⁴⁵Horia Hulubei National Institute of Physics and Nuclear Engineering, Bucharest, Romania
⁴⁶Indian Institute of Technology Bombay (IIT), Mumbai, India
⁴⁷Indian Institute of Technology Indore, Indore, India
⁴⁸INFN, Laboratori Nazionali di Frascati, Frascati, Italy

- ⁴⁹*INFN, Sezione di Bari, Bari, Italy*
- ⁵⁰*INFN, Sezione di Bologna, Bologna, Italy*
- ⁵¹*INFN, Sezione di Cagliari, Cagliari, Italy*
- ⁵²*INFN, Sezione di Catania, Catania, Italy*
- ⁵³*INFN, Sezione di Padova, Padova, Italy*
- ⁵⁴*INFN, Sezione di Pavia, Pavia, Italy*
- ⁵⁵*INFN, Sezione di Torino, Turin, Italy*
- ⁵⁶*INFN, Sezione di Trieste, Trieste, Italy*
- ⁵⁷*Inha University, Incheon, Republic of Korea*
- ⁵⁸*Institute for Gravitational and Subatomic Physics (GRASP), Utrecht University/Nikhef, Utrecht, Netherlands*
- ⁵⁹*Institute of Experimental Physics, Slovak Academy of Sciences, Košice, Slovak Republic*
- ⁶⁰*Institute of Physics, Homi Bhabha National Institute, Bhubaneswar, India*
- ⁶¹*Institute of Physics of the Czech Academy of Sciences, Prague, Czech Republic*
- ⁶²*Institute of Space Science (ISS), Bucharest, Romania*
- ⁶³*Institut für Kernphysik, Johann Wolfgang Goethe-Universität Frankfurt, Frankfurt, Germany*
- ⁶⁴*Instituto de Ciencias Nucleares, Universidad Nacional Autónoma de México, Mexico City, Mexico*
- ⁶⁵*Instituto de Física, Universidade Federal do Rio Grande do Sul (UFRGS), Porto Alegre, Brazil*
- ⁶⁶*Instituto de Física, Universidad Nacional Autónoma de México, Mexico City, Mexico*
- ⁶⁷*iThemba LABS, National Research Foundation, Somerset West, South Africa*
- ⁶⁸*Jeonbuk National University, Jeonju, Republic of Korea*
- ⁶⁹*Fachbereich Informatik und Mathematik, Johann-Wolfgang-Goethe Universität Frankfurt Institut für Informatik, Frankfurt, Germany*
- ⁷⁰*Korea Institute of Science and Technology Information, Daejeon, Republic of Korea*
- ⁷¹*KTO Karatay University, Konya, Turkey*
- ⁷²*Laboratoire de Physique des 2 Infinis, Irène Joliot-Curie, Orsay, France*
- ⁷³*Laboratoire de Physique Subatomique et de Cosmologie, Université Grenoble-Alpes, CNRS-IN2P3, Grenoble, France*
- ⁷⁴*Lawrence Berkeley National Laboratory, Berkeley, California, USA*
- ⁷⁵*Division of Particle Physics, Department of Physics, Lund University, Lund, Sweden*
- ⁷⁶*Nagasaki Institute of Applied Science, Nagasaki, Japan*
- ⁷⁷*Nara Women's University (NWU), Nara, Japan*
- ⁷⁸*Department of Physics, School of Science, National and Kapodistrian University of Athens, Athens, Greece*
- ⁷⁹*National Centre for Nuclear Research, Warsaw, Poland*
- ⁸⁰*National Institute of Science Education and Research, Homi Bhabha National Institute, Jatni, India*
- ⁸¹*National Nuclear Research Center, Baku, Azerbaijan*
- ⁸²*National Research and Innovation Agency - BRIN, Jakarta, Indonesia*
- ⁸³*Niels Bohr Institute, University of Copenhagen, Copenhagen, Denmark*
- ⁸⁴*Nikhef, National Institute for Subatomic Physics, Amsterdam, Netherlands*
- ⁸⁵*Nuclear Physics Group, STFC Daresbury Laboratory, Daresbury, United Kingdom*
- ⁸⁶*Nuclear Physics Institute of the Czech Academy of Sciences, Husinec-Řež, Czech Republic*
- ⁸⁷*Oak Ridge National Laboratory, Oak Ridge, Tennessee, USA*
- ⁸⁸*Ohio State University, Columbus, Ohio, USA*
- ⁸⁹*Physics department, Faculty of science, University of Zagreb, Zagreb, Croatia*
- ⁹⁰*Physics Department, Panjab University, Chandigarh, India*
- ⁹¹*Physics Department, University of Jammu, Jammu, India*
- ⁹²*Physics Program and International Institute for Sustainability with Knotted Chiral Meta Matter (SKCM2), Hiroshima University, Hiroshima, Japan*
- ⁹³*Physikalisches Institut, Eberhard-Karls-Universität Tübingen, Tübingen, Germany*
- ⁹⁴*Physikalisches Institut, Ruprecht-Karls-Universität Heidelberg, Heidelberg, Germany*
- ⁹⁵*Physik Department, Technische Universität München, Munich, Germany*
- ⁹⁶*Politecnico di Bari and Sezione INFN, Bari, Italy*
- ⁹⁷*Research Division and ExtreMe Matter Institute EMMI, GSI Helmholtzzentrum für Schwerionenforschung GmbH, Darmstadt, Germany*
- ⁹⁸*Saga University, Saga, Japan*
- ⁹⁹*Saha Institute of Nuclear Physics, Homi Bhabha National Institute, Kolkata, India*
- ¹⁰⁰*School of Physics and Astronomy, University of Birmingham, Birmingham, United Kingdom*
- ¹⁰¹*Sección Física, Departamento de Ciencias, Pontificia Universidad Católica del Perú, Lima, Peru*
- ¹⁰²*Stefan Meyer Institut für Subatomare Physik (SMI), Vienna, Austria*
- ¹⁰³*SUBATECH, IMT Atlantique, Nantes Université, CNRS-IN2P3, Nantes, France*
- ¹⁰⁴*Sungkyunkwan University, Suwon City, Republic of Korea*
- ¹⁰⁵*Suranaree University of Technology, Nakhon Ratchasima, Thailand*
- ¹⁰⁶*Technical University of Košice, Košice, Slovak Republic*

- ¹⁰⁷*The Henryk Niewodniczanski Institute of Nuclear Physics, Polish Academy of Sciences, Cracow, Poland*
- ¹⁰⁸*The University of Texas at Austin, Austin, Texas, USA*
- ¹⁰⁹*Universidad Autónoma de Sinaloa, Culiacán, Mexico*
- ¹¹⁰*Universidade de São Paulo (USP), São Paulo, Brazil*
- ¹¹¹*Universidade Estadual de Campinas (UNICAMP), Campinas, Brazil*
- ¹¹²*Universidade Federal do ABC, Santo Andre, Brazil*
- ¹¹³*University of Cape Town, Cape Town, South Africa*
- ¹¹⁴*University of Houston, Houston, Texas, USA*
- ¹¹⁵*University of Jyväskylä, Jyväskylä, Finland*
- ¹¹⁶*University of Kansas, Lawrence, Kansas, USA*
- ¹¹⁷*University of Liverpool, Liverpool, United Kingdom*
- ¹¹⁸*University of Science and Technology of China, Hefei, China*
- ¹¹⁹*University of South-Eastern Norway, Kongsberg, Norway*
- ¹²⁰*University of Tennessee, Knoxville, Tennessee, USA*
- ¹²¹*University of the Witwatersrand, Johannesburg, South Africa*
- ¹²²*University of Tokyo, Tokyo, Japan*
- ¹²³*University of Tsukuba, Tsukuba, Japan*
- ¹²⁴*University Politehnica of Bucharest, Bucharest, Romania*
- ¹²⁵*Université Clermont Auvergne, CNRS/IN2P3, LPC, Clermont-Ferrand, France*
- ¹²⁶*Université de Lyon, CNRS/IN2P3, Institut de Physique des 2 Infinis de Lyon, Lyon, France*
- ¹²⁷*Université de Strasbourg, CNRS, IPHC UMR 7178, F-67000 Strasbourg, France, Strasbourg, France*
- ¹²⁸*Département de Physique Nucléaire (DPhN), IRFU, Université Paris-Saclay Centre d'Etudes de Saclay (CEA), Saclay, France*
- ¹²⁹*Università degli Studi di Foggia, Foggia, Italy*
- ¹³⁰*Università del Piemonte Orientale, Vercelli, Italy*
- ¹³¹*Università di Brescia, Brescia, Italy*
- ¹³²*Variable Energy Cyclotron Centre, Homi Bhabha National Institute, Kolkata, India*
- ¹³³*Warsaw University of Technology, Warsaw, Poland*
- ¹³⁴*Wayne State University, Detroit, Michigan, USA*
- ¹³⁵*Westfälische Wilhelms-Universität Münster, Institut für Kernphysik, Münster, Germany*
- ¹³⁶*Wigner Research Centre for Physics, Budapest, Hungary*
- ¹³⁷*Yale University, New Haven, Connecticut, USA*
- ¹³⁸*Yonsei University, Seoul, Republic of Korea*
- ¹³⁹*Zentrum für Technologie und Transfer (ZTT), Worms, Germany*
- ¹⁴⁰*Affiliated with an institute covered by a cooperation agreement with CERN*
- ¹⁴¹*Affiliated with an international laboratory covered by a cooperation agreement with CERN*

^aAlso at Max-Planck-Institut für Physik, Munich, Germany.

^bAlso at Italian National Agency for New Technologies, Energy and Sustainable Economic Development (ENEA), Bologna, Italy.

^cAlso at Dipartimento DET del Politecnico di Torino, Turin, Italy.

^dDeceased.

^eAlso at An institution covered by a cooperation agreement with CERN.

^fAlso at Department of Applied Physics, Aligarh Muslim University, Aligarh, India.

^gAlso at Institute of Theoretical Physics, University of Wrocław, Poland.